INFORMATION TO USERS

This manuscript has been reproduced from the microfilm master. UMI films the text directly from the original or copy submitted. Thus, some thesis and dissertation copies are in typewriter face, while others may be from any type of computer printer.

The quality of this reproduction is dependent upon the quality of the copy submitted. Broken or indistinct print, colored or poor quality illustrations and photographs, print bleedthrough, substandard margins, and improper alignment can adversely affect reproduction.

In the unlikely event that the author did not send UMI a complete manuscript and there are missing pages, these will be noted. Also, if unauthorized copyright material had to be removed, a note will indicate the deletion.

Oversize materials (e.g., maps, drawings, charts) are reproduced by sectioning the original, beginning at the upper left-hand corner and continuing from left to right in equal sections with small overlaps.

ProQuest Information and Learning
300 North Zeeb Road, Ann Arbor, MI 48106-1346 USA
800-521-0600

University of Alberta

Fluid Properties of Asphaltenes at 310 – 530 °C

by

Oswaldo Jose Asprino Brinez 

A thesis submitted to the Faculty of Graduate Studies and Research in partial fulfillment of the requirements for the degree of Master of Science

in

Chemical Engineering

Department of Chemical and Materials Engineering

Edmonton, Alberta

Spring, 2005

ABSTRACT

Thermal cracking processes are used extensively in the conversion of the vacuum residue fraction of Athabasca bitumen (AVR). The fluid properties of surface tension, viscosity, and contact angle of the reacting bitumen are important in fouling of equipment and for adhesion during cracking in fluidized beds. Cracking processes can operate downstream of other units, which alter the boiling distribution and asphaltene content of the feed. In this work, the role of composition on fluid properties is investigated at temperatures 312 – 530 °C by varying the contents of asphaltenes and bitumen solids. The results for the AVR-asphaltenes are compared with results for other asphaltenes. Viscosity and surface tension of AVR-asphaltenes were higher than whole AVR for at all temperatures. These properties were not affected by the solids. The contact angle of molten asphaltenes on different surfaces indicated that the wettability on coke was better than on a Ni/Fe alloy.

ACKNOWLEDGEMENT

I would like to thank Dr. Murray Gray for patiently helping and guiding me along this new and exciting learning experience.

To Dr. William McCaffrey for his help, opportune advice, and professional friendship.

To the advanced bitumen upgrading group and the support staff of the Chemical and Material Engineering department, specially Tuyet, Leanne, and AnnMarie.

To my mother Corina, my wife Janeth, my brother Jorge and all my family who always trusted in me, even from far away you motivated me during this journey.

To Pedro and Eli for your friendship and for letting me enjoy and take advantage of your enormous thirst of knowledge.

To my all-around-the-world-friends and fellows who in one way or another participated in this work

To those who I truly admire, without knowing, they have inspired me.

And finally I would like to acknowledge the Syncrude Canada Ltd. and the National Science and Engineering Research Council of Canada Industrial Research Chair in Advanced Upgrading of Bitumen for the financial support of this project.

TABLE OF CONTENTS

LIST OF TABLES

LIST OF FIGURES

NOMENCLATURE

AVR	Athabasca vacuum residue
D	Distance between the rods or liquid bridge length, mm
dD/dt	Rate of separation of the rods, mm/s
$d\gamma/dT$	Surface tension temperature coefficient, mN/(m °C)
e_1, e_2	Constants for the various temperatures of interest
F_{mag}	Force due to the magnetic field effect, mN
F_T	Total force, mN
h	Height of the liquid drop , cm (Equation 2-3)
h_L	Absolute position of the free (lower) rod, cm
h_u	Absolute position of the controlled (upper) rod, cm
L	Length of the sprayed portion of the alloy rod, cm
LVDT	Linear variable displacement transducer
m_{coated}	Mass of the assembly after spraying and drying, g (Equation 3-1)
m_{dry}	Mass of the assembly before spraying and taping, g (Equation 3-1)
$m_{t=0}$	Initial mass of coat on the road
$m_{t=\infty}$	Final mass of coat on the road

R	Radius of the alloy rod, mm
r	Radius of the liquid drop, cm (Equation 2-3)
T	Temperature, °C
t	Reaction time, s (Equation 2-6)
t_s	Heating time at the point of commencement of bridge elongation, s
t_t	Time to touch rods (heating time from the when furnace was turned on till rods touched), s
t_v	Heating time at the maximum elongation of the bridge, s
V_L	Voltage reading from the equipment for the controlled rod, V
V_u	Voltage reading from the equipment for the free rod, V
V_{eq}	Voltage reading of the free rod at equilibrium point, V
VR	Vacuum residue
X	Initial content of asphaltenes, wt % s
$X_{m,\,t=\infty}$	Fraction of mass that remains in the rod no at t = ∞
X_{ext}	Fraction of extractable material converted at a time t
X_S	Weight fraction of solids in the mixture
x	Molar, mass or volume fraction

Greek Symbols

θ	Contact angle, ° (Equation 2-3)
γ	Surface tension of the liquid, mN/m
γ_s	Surface tension of the solid surface, mN/m
γ_{sl}	Interfacial tension between the liquid and the solid surface, mN/m
λ	Viscosity interaction parameter
μ	Viscosity, Pa.s
δ	Film thickness of the thin coating the rods, mm
ρ	Density of the liquid of interest, kg/m^3
ρ_M	Density of the mixture, kg/m^3
ρ_S	Density of the solid, kg/m^3
τ_R	Relaxation time of the dynamic contact angle, s (Equation 4-4)

Sub Scripts

$t = 0$	Initial stage
$t = \infty$	Final stage
i, j, k	Component indexes

1. INTRODUCTION

1.1 RESEARCH BACKGROUND

The enormous resources of oilsands bitumen in Western Canada require extensive processing in order to produce transportation fuels, particularly the vacuum residue fraction which makes up 50 – 60 % by weight of the extractable oil. This property has led to the extensive use of cracking processes to convert and recover valuable products from the residue remaining after vacuum distillation.

The upgrading of bitumen and petroleum residue to distilled products is achieved by either thermal coking or catalytic hydroconversion. In both processes, the yield of products is controlled partially by a proper feeding and contact between feed and fluidized bed or feed and catalyst. Hence, it is important to control or manage the optimum conditions of feeding, recycling, etc. to improve the operability and efficiency of the units. These goals are only achievable through a better understanding of the properties of the fluids involved. Three key properties are surface tension, viscosity, and contact angle.

Upgrading processes, such as cokers, can operate downstream of distillation or deasphalting units, which alter the boiling distribution and asphaltene content of the feed. Consequently, the fluid properties of the reacting bitumen need to be measured for different feed compositions. Athabasca bitumen and its vacuum residue contain significant amounts of asphaltenes, in the range of 10 – 30 wt %, therefore an understanding of asphaltenes properties will help to develop an

understanding of the global properties of bitumens and residues (Rahmani, 2003a). Another important but unstudied compositional variable for the fluid proprieties of the Athabasca vacuum residue is the possible but unlikely influence of the fine mineral solids present in the bitumen.

Fluid properties of the reacting bitumen and its constituents are very important not only for the operability and efficiency of processes, but also for the design of equipment and mitigation of fouling. Information on fluid properties as a function of reaction time are necessary to allow design of improved feed systems and to optimize the residence time distribution. Fouling of process vessels and heat-transfer equipment is a major concern in processing these heavy oils and bitumens, due to higher fuel consumptions and the operational costs of removing deposits from equipment. Asphaltenes play an important role in fouling of equipment, through mechanisms that include liquid-phase instability and coke formation.

The operating temperatures of the commercial coking processes are severe, in the range of 450 – 550 °C. However, to obtain a better sense of the behavior of the fluid properties at high temperature not only do the properties need to be measured at reaction conditions but also at lower temperatures (300 – 450 °C). The lower temperature regime would bring also insight regarding the fluid properties of the materials before the thermal cracking reactions regime. The lower temperature regime is closer to the temperatures used in the upstream processes such as distillation columns, heat exchangers, etc.

1.2 RESEARCH OBJECTIVES

The objectives of this work are:

- Study the effect of composition on the fluid properties of the Athabasca vacuum residue, using asphaltenes as a convenient extreme case
- Compare the fluid properties of Athabasca vacuum residue asphaltenes with fluid properties of other asphaltenes (from Asia, Middle East, N. America)
- Study the influence of the fine solids in the fluid properties of the Athabasca vacuum residue

The fluid properties to be measured in this work are:

- Surface tension
- Viscosity
- Contact angle

2. LITERATURE REVIEW

In this chapter, the theoretical background will be discussed in order to lay the basis for this thesis. The definitions of bitumen and vacuum residue as well as the characteristics and properties of their components will be reviewed. A definition for asphaltenes is provided in this chapter that will be used throughout the thesis. Finally, the liquid bridge technique as a means to measure surface tension and viscosity at high temperatures is explained.

2.1 ATHABASCA BITUMEN AND VACUUM RESIDUE

Bitumen is a complex mixture of hundreds of high molecular weight compounds. It has a viscosity of > 100 Pa.s at 15 °C and a density > 1000 kg/m^3 (< 10 °API). Athabasca bitumen is rich in heteroatoms such as sulfur and nitrogen; and in metals such as vanadium and nickel. Bitumen from surface mining operations also has a high fine-solids content that will be explained later in Section 2.1.1. Approximately 50 % of the bitumen can be recovered by vacuum distillation, the remaining 50 % is called vacuum residue (VR). Another common definition for the vacuum residue is the fraction boiling above 524 °C (524 °C+), based on its atmospheric equivalent boiling point. The properties of the Athabasca vacuum residue (AVR) are shown in Table 2-1.

Table 2-1. Characteristics of Athabasca Vacuum Residue (AVR)
(Gray et al., 2001 and Gray et al., 2004b)

Characteristic	
Toluene insoluble, wt%	1.8
n-C_7-insoluble asphaltenes, wt %	31.4
MCR, wt %	27.8
Aromatic Carbon, %	38.7
Sulfur, wt %	5.72
Nitrogen, wppm	7206
Density, kg/m^3 @ 20 °C	1087
Boiling fraction, wt %	
524 °C -	10
524-650 °C	40
650 °C +	50

The characterization of the bitumen and vacuum residue usually involves division into several fractions or components. The two major fractions, separated based on their solubility in either *n*-pentane or *n*-heptane, are maltenes and asphaltenes. The soluble maltenes are further subdivided in distillables and non-distillables using a defined cut-off temperature of 524 °C. Athabasca bitumen and the VR contain significant amounts of *n*-heptane insoluble asphaltenes, in the range of 10 – 30 wt % (Rahmani, 2003a).

2.1.1 PROCESS FOR BITUMEN CONVERSION

In order to make use of the vacuum residue for manufacture of transportation fuels, upgrading technologies have to be applied. The two major processes to accomplish this primary upgrading step are coking and hydroconversion. Two major coking processes are available: fluid coking and delayed coking. Both processes are carried out at temperatures 430 – 550 °C and low pressures (100 – 350 kPa).

In the fluid coking process (according to the Syncrude Canada Ltd.), the liquid feed is a mixture of atmospheric topped bitumen, vacuum residue, and residuum from the LC-Finer (hydroconversion unit for moderate conversion). This feed at 350 °C is sprayed into a fluidized bed of fine coke particles at 510 – 540 °C. The feed reacts on the surface of the hot coke particles producing light gas, naphtha and gas oil. Within this process, surface tension, viscosity and the kinetics of reaction will determine how the feed spreads on coke particles, how particles agglomerate, and the rate of fouling in the reactor.

In delayed coking, the liquid feed is heated in a furnace to 490 – 510 °C then injected into a large, open vessel where the cracking reactions occur and the coke accumulates. The vapor products (light gases), naphtha and gas oil, exit at the top of the vessel. The viscosity and contact angle of asphaltenic material may be related to fouling of furnace tubes. Surface tension and viscosity of reacting liquid will likely determine the morphology of the coke product (Gray, 2002).

Both processes, fluid and delayed coking, strip off volatiles, leaving heavy component to react in the liquid phase. In contrast, hydroconversion occurs in a liquid environment where the product remains as a solvent for heavy components, along with high concentration of dissolved hydrogen at > 10 MPa and 410 – 440 °C and the presence of catalyst. The focus of this thesis will be properties under low pressure conditions for coking.

2.1.2 Bitumen Solids in Athabasca Vacuum Residue (AVR)

The Athabasca bitumen, produced by surface mining and conventional froth treatment with a naphtenic diluent, contains a considerable amount of filterable solids. These fine solids are originally present in the commercially produced Athabasca bitumen as mineral clays coated with strongly bound toluene-insoluble organic materials. The concentration of these solids in the Athabasca bitumen is approximately 0.9 wt%, and approximately 1.8 wt% in the Athabasca vacuum residue (AVR) (Kotlyar et al. 1999). The type and amount of fine solids depends on the origin and grade of the oil sand. Budziak et al. (1988) found that the bitumen-solids are composed of mineral clays, mainly kaolinite and illite, and sand grains (mostly SiO_2 and feldspar).

According to Tanabe and Gray (1997) these bitumen-solids affect the coalescence of toluene-insoluble material at the early stages of coking reactions. They showed that these fine solids inhibited the formation of toluene-insoluble coke from AVR during coking reactions. Bitumen-solids are also associated with

corrosion and fouling problems caused by the high chloride content of the salt residues, and to coke formation in catalyst and in consequence plugging of hydrotreaters (Kotlyar et al. 1999).

2.2 ASPHALTENES

Asphaltenes are a solubility class in petroleum and coal liquids and not a pure component. They are defined as the part of the crude oil that is soluble in toluene and insoluble in *n*-pentane or *n*-heptane. They consist of many chemical species and their composition is not well defined. Asphaltenes appear to interact with each other and with other oil constituents in a complex manner. Vapor pressure osmometry (VPO) studies have demonstrated that different molar masses are observed at different asphaltene concentrations, temperatures, and solvents due to molecular association (Yarranton, et al. 2000). Chemical properties and the concentrations of the different carbon types in *n*-C_7-insoluble asphaltenes are given in Tables 2-2 and 2-3.

Table 2-2. Chemical characteristics of n-C_7-insoluble asphaltenes
(Rahmani et al., 2003a)

Sample	H/C Ratio	Sulfur, wt %	Sulfide S, wt %	Nitrogen, wt %
Athabasca VR	1.19	7.47	3.78	1.28
Maya VR[1]	-	7.1	-	1.31
Arab Heavy VR	1.16	7.15	3.27	0.92
Gudao VR	1.41	4.44	2.28	1.18

[1] Data from Microanalytical laboratory of the Chemistry Dept. University of Alberta

Table 2-3. Concentration of representative carbon types in n-C_7-insoluble asphaltenes from NMR
(Rahmani et al., 2003a)

Carbon Types	Athabasca VR	Maya[1]	Arab Heavy VR	Gudao VR
	Percent of total carbon ,% C_{tot}			
Total aromatic (f_a)	55	53	52	40
Paraffin CH	8.6	8.3	11.4	10.6
Paraffin CH_2, > 5 C	8.2	8.1	8.9	16.7
Terminal paraffinic methyl	2.3	2.8	2.3	2.9
Cycloparaffinic CH_2	4.7	3.8	3.7	5.1
Aromatic CH_3	2.4	2.2	2.3	2.2
Cylcoparaffinic CH_3	3.5	3.6	2.9	3.8

[1] Note that these data are for Maya crude and not for Maya vacuum residue

Based on data from MNR, elemental analysis and selective oxidation and thermal degradation, Sheremata et al. (2004) proposed models for the Athabasca asphaltenes with and archipelago structure, like the one shown in Figure 2-1. They also justified this kind of model from the fact that any model for the asphaltene chemical structure must be consistent with the observed characteristics of products from upgrading processes. The other model proposed for the asphaltene molecules consist of a pericondensed structure at the core of > 7 fused rings, with pendant aliphatic groups. When asphaltenes are pyrolysed, a full range of products arises in the naphtha (C_5 – 177 °C), gas oil (343 – 524 °C), and residue (524 °C+) fractions. Pyrolysis of pericondensed asphaltenes would yield products only in the gas, naphtha and residue fractions (Sheremata et al., 2004).

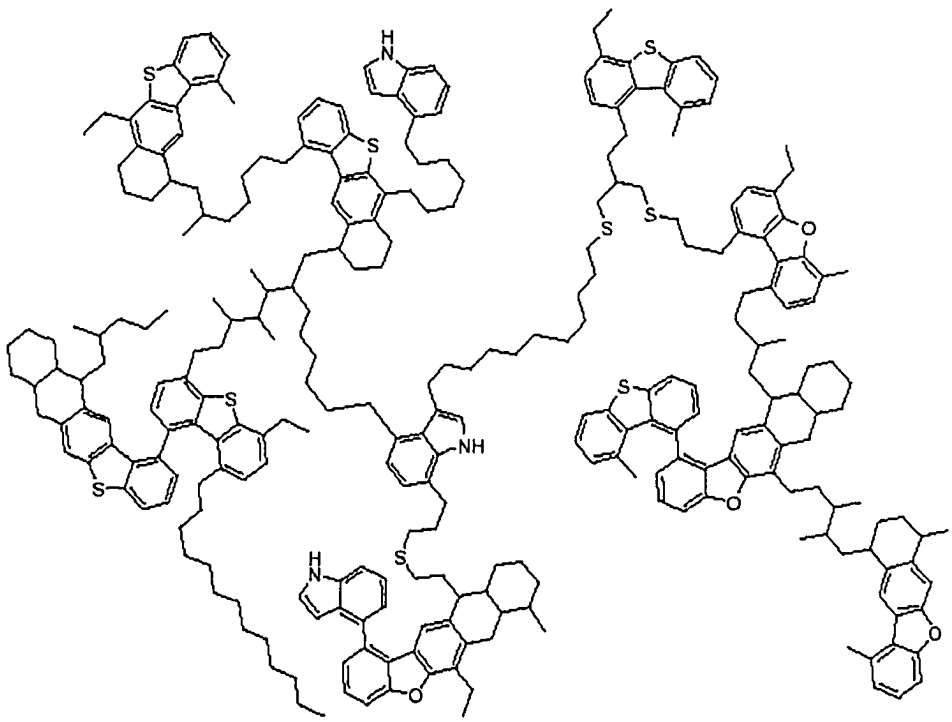

Figure 2-1. Asphaltene molecular representation (Sheremata et al., 2004)

Asphaltene content is an important indicator for refinery processing and upgrading of bitumens. The amount of asphaltene correlates to some degree with yield of coke in delayed cokers and coke deposition in hydroconversion catalyst (Gray et al. 2004a). Asphaltenes also play an important role in fouling of equipment, through mechanisms that include liquid-phase instability and coke formation (Gray et al., 1999). Their deposition on solid surfaces may be controlled by the wetting and adhesion of asphaltenic liquids on solid surfaces. Watkinson and Wilson (1997) and Watkinson and Asomaning (2000) discussed the role of the asphaltenes in the fouling of heat exchangers, claiming that the precipitated asphaltenes adhere to the hot surface of the exchanger and then carbonize into coke. They found that higher asphaltene content in solution does not necessarily correlate with increasing fouling. Rather, the fouling rates increased with surface temperature and increasing flow velocity, suggesting the importance of an adhesion step in the fouling mechanism.

The changes of the wettability caused by asphaltenes have been studied under various conditions, and all the findings indicate that the asphaltenes do change the surface properties of solids. Gloton et al. (1992), and Akhlaq et al. (1997) measured the change of the wettability caused by the asphaltene adsorption on glasses in contact with of glycerol and dioctylphtalate at room temperature. They concluded that the absorption of asphaltenes, from a good solvent such as toluene, irreversibly changes the original hydrophilic properties of the glasses. Buckley (2001), and Al-Maamari and Buckley (2003) discussed the alteration of

the wettability of mineral solid surfaces by asphaltenes with an aqueous phase present at low temperatures, concluding that the asphaltenes alter wetting mechanisms such as ionic interactions and surface precipitation. Despite the possible role of adhesion in fouling by asphaltenes in heat transfer equipments, as suggested by Watkinson and Asomaning (2000), contact angle of "pure" asphaltenes under conditions closer to the industrial processes has not been studied.

2.2.1 ASPHALTENES AS LIQUIDS

At elevated temperatures, recent research by Gray et al. (2004a) suggests that asphaltenes are likely liquid fluid at process temperatures, even in the absence of other oil components to serve as solvents. However, as a complex mixture of components, asphaltenes may not display a distinct melting point (Gray et al. 2004a). According to Kopsch (1994), no information on melting of asphaltenes is available on the technical literature because asphaltenes are assumed to pyrolyze below the estimated melting temperatures. Nevertheless, Kopsch (1994) reported glass transition temperatures for Kirkuk asphaltenes between 313 – 350 °C using a differential scanning calorimeter and a heating rates between 10 and 50 °C/min. Zhang et al. (2004) also reported glass transition temperatures for asphaltenes of 120 – 130 °C using a differential scanning calorimeter and a heating rate of circa 0.17 °C/s. Gray et al. (2004a) observed melting behavior when heating thin films of different asphaltenes on Curie-point alloy strips. They worked at a significantly higher heating rate of 16.5 °C/s, which is much closer to the real industrial

processes were the asphaltenes are involved. The results of Gray et al. (2004a) are presented in Table 2-4.

Table 2-4. Temperatures of melt formation from asphaltene samples
(Gray et al., 2004a)

Sample	Average temperature (n = 3), °C	Standard Deviation, °C
Athabasca VR	224	16
Maya VR	294	16
Arab Heavy VR	245	29
Gudao VR	< 275*	--

*Liquid behavior was observed at this temperature (275 °C)

2.3 Fluid Properties of Athabasca Bitumen, AVR and Asphaltenes

2.3.1 Surface Tension

For liquids, the surface tension is the specific free surface energy, equivalent to a line tension acting in all directions parallel to the surface. Thermodynamically, the surface tension is the work to be done per unit of area of surface extension. Within the liquid, the surface tension manifests itself as an internal force, which tends to reduce the external surface area to a minimum (Van Krevelen, 1997).

Many studies have looked at the surface tension of bitumen, mainly examining the influence of temperature, composition, and surfactants at low temperature. Isaacs and Smolek (1983) measured the interfacial tension of Athabasca bitumen in contact with aqueous surfactants between 50 and 150 °C. Potoczny et al. (1984) measured the surface tension of Alberta bitumens between 40 and 90 °C. Potoczny et al. (1984) discussed the change of the surface tension and its temperature coefficient ($d\gamma/dT$) with factors such as the molecular weight and the length of the molecular chains. Other papers used surface tension measurements as a means of determining other properties of the mixtures such as critical micelle concentration, state of aggregation, colloidal behavior, etc. (Sheu et al., 1992; Rogel et al., 2000; Yarranton et al. 2000; and Da Silva Ramos et al., 2001). All these studies showed that the surface tension of dilute mixtures of bitumen/asphaltenes decreased with the weight fraction of asphaltenes. Two studies have measured surface tension of vacuum residue at elevated temperatures. Li et al. (2003) measured the surface tension between 150 and 280 °C using the pendant drop technique. They reported dynamic and equilibrium values of the surface tension in the range of 20 – 25 and 18 – 21 mN/m, respectively. Aminu (2003) and Aminu et al. (2004) worked at higher temperatures, between 312 and 530 °C. They reported dynamic surface tensions measured using the liquid bridge technique in the range of 5 – 15 mN/m.

A very important factor affecting the properties of AVR may be the presence of bitumen-solids. The influence of the solid particles on the surface

tension was the subject of the work by Brian and Chen (1987). They worked at 20 °C with solid-liquid slurries, loading the system with particles from 0.5 up to 106 μm and loads from 0 to 45 wt%. Brian and Chen (1987) found that the surface tension remained constant within an experimental scatter of 3 %. Vargha-Butler et al. (1988) investigated the effect of clays on the surface tension of Alberta bitumens between 40 and 90 °C. The surface tension measured by Vargha-Butler et al. (1988), using a Wilhelmy plate, was independent of the presence of clays. In the same range of temperature (40 – 90 °C), Drelich et al. (1994) measured the surface tension of bitumen extracted from Utah oil sands, taking into consideration also the role of clays. They claimed that the differences observed when calculating the surface tension from contact angle measurements were probably not due to the clay particles. Because these studies concluded that the solids or clays did not affect the surface tension at 20 – 90 °C, we would not expect fine solids to influence the surface tension of AVR at higher process temperatures.

In addition to the work done on measuring the surface tension, some other papers proposed models to predict this property. Mehrotra at al. (1985) discussed the suitability of the principle of correspondent states (PCS) and the Rice-Teja methods to predict the surface tension of Athabasca bitumen between 64 and 112 °C. They obtained deviation from –5 and –12 % with respect to the experimental data. Both proposed methods require experimental data and acentric factors. Additionally, the PCS method needs the characterization of the bitumen in terms of critical properties.

Except for the work of Aminu (2003) and Aminu et al. (2004), no other results on the surface tension of AVR have been reported for temperatures > 300 °C. Data for asphaltenes are even scarcer. The only data available are for much lower temperatures for diluted systems where the asphaltenes are just one more component. This lack of data is likely due to the limitations of the commercial equipment for measuring the surface tension, which are the limited temperature range and the inability to handle reacting systems, with vapors or volatile products being generating during the measurements.

2.3.2 Viscosity and Rheology

Viscosity is defined as ratio of the shear stress per unit area at any point in a confined fluid to the velocity gradient in the direction perpendicular to the direction of flow (Perry, 1999). The viscosity can also be considered as a measure of momentum conductivity, analogous to the thermal conductivity in heat transfer (Streeter, 1961).

At relatively low temperatures, the viscosity of bitumens and vacuum residues can be easily measured. For this reason a number of papers have been published and data are available for the viscosity of bitumen at low temperatures (room temperature to 100 °C). According to Schramm and Kwak (1988) and Khan et al. (1984), bitumen can be considered Newtonian above 80 °C for any practical purposes. Schramm and Kwak (1988) only observed some non-Newtonian character for some bitumens and heavy oils at very low shear rates regimes

(0 - 1 s^{-1}). More recently, Storm et al. (1991) also observed Newtonian behavior for mixtures of deasphalted oil and asphaltenes at 93 °C. The rheology and Newtonian character of the AVR have not been formally studied. According to Aminu (2003), many studies already done regarding the rheology of bitumen have indicated that AVR will exhibit Newtonian behavior at temperatures > 200 °C. In the case of asphaltenes, there is no reason to expect significant departure from the behavior of a Newtonian liquid at elevated temperatures.

Several authors have studied or commented on the influence of asphaltenes on the viscosity. Altgelt and Harle (1975) studied the effect of the asphaltenes on the viscosity of asphalts using a pressurized capillary viscometer. Dealy (1979), Werner et al. (1998b), and Rayes et al. (2002) worked with different mixtures between 25 and 100 °C. All agreed on the strong effect of the asphaltenes in increasing the viscosity of the bitumen or heavy oil. Werner et al. (1998a) reported a value for the viscosity of asphaltenes of 8.589 mPa.s. They warned about this value of viscosity and clearly stated that it was calculated by fitting of the experimental data. In consequence, this value was only a parameter that represents the influence of the asphaltenes in their model, not the real viscosity of the asphaltenes without the other components in the oil.

The only published works where the viscosity of AVR has been measured above 300 °C are Aminu (2003) and Aminu et al. (2004). Aminu (2003) measured the viscosity of AVR at temperatures between 185 and 530 °C, and Aminu et al.

(2004) between 400 and 530 °C. They reported significant changes of the viscosity with the temperature. Their results are presented later in Chapter 4 for comparison.

No data or publications could be found regarding viscosity of non-diluted or solvent-free asphaltenes at high temperatures, i.e. above 300 °C. The same limitations mentioned in Section 2.3.1, due to the high temperature and measurements of reacting systems, apply for determining the viscosity of asphaltenes.

Models to correlate and/or to predict the viscosity of bitumens have been extensively studied, giving attention to factors such as the influence of temperature, pressure and dissolved gas. Mehrotra et al. (1996) published a complete review of most of the calculation methods for the viscosity of liquid hydrocarbons and their mixtures. They stated in the conclusions that most of the existing methods required viscosity data to determine one or more adjustable parameters and, in the case of mixtures, interaction parameters are also needed. After the publication of the review of Mehrotra et al. (1996), some other models were proposed for the viscosity of heavy oils and bitumens, among them Miadonye, et al. (1997, 2001) and Bryan et al. (2003). The latter took a completely different approach based on nuclear magnetic resonance relaxometry. Correlations to calculate the viscosity of some bitumens as a function of its liquid fractions and blended with diluents have been proposed by Khan et al. (1984), Mehrotra et al. (1989), and Mehrotra (1992). The correlation used in most of the cases for the liquid mixture viscosity is of the form of equation 2-1.

$$\ln(\mu_m) = \sum_{i=1}^{n} x_i \ln(\mu_i) \qquad (2\text{-}1)$$

In this equation x may stand for volume, molar or weight fraction, the sub script m stands for mixture, and i for the component i in the mixture (Mehrotra et al., 1989). Usually interaction parameters are used in equation 2-1 (Mehrotra, 1992), giving more complex equations like the one shown in Equation 2-2, used by Werner et al. (1998a), where the parameters λ_{ij} are the binary, and λ_{ijk} are the ternary interaction coefficients.

$$\ln(\mu_m) = \sum_{x_i} \ln \mu_i + \sum_{i} \sum_{j \neq i} x_i x_j \lambda_{ij} + \sum_{i} \sum_{j \neq i} \sum_{k \neq i,j} x_i x_j x_k \lambda_{ijk} + \ldots \qquad (2\text{-}2)$$

Another alternative found in the literature for the calculation of the viscosity of bitumens is the extended corresponding states method (Johnson et al., 1987), but this method requires the characterization of the bitumen in terms of its critical properties and acentric factor (Mehrotra et al., 1989). Alternatively, the required parameter for the extended corresponded states method could be calculated empirically (Khan et al., 1984). Werner et al. (1998a) proposed a more complete model for the calculation of viscosity of petroleum systems with high asphaltene contents. They include the effect of pressure, temperature and composition of pseudocomponents in the model, which only requires the knowledge of the viscosity of the mixture at a reference state. The model was limited for pressures between 0.1 and 29 MPa and temperatures between 31 to 84.5 °C.

In regards to the influence of bitumen-solids in the AVR on the viscosity, no special attention has been paid to this issue. Only Schramm and Kwak (1988) recognized the presence of the solids during the viscosity measurements of Athabasca bitumen, but did not make any effort to study its influence.

2.3.3 CONTACT ANGLE

The degree to which a liquid wets a solid is measured by the contact angle. When the contact angle approaches zero, the liquid spreads freely over the surface and is said to completely wet it. This occurs when the molecular attraction between the liquid and solid molecules is greater than that between similar liquid molecules (Gent and Hamed, 2002).

One of the most frequently used equations to define the contact angle is the Young equation, Equation 2-3. In this equation, γ_s is the surface tension of the solid surface, γ_{sl} is the interfacial tension between the liquid and the solid, and γ is the surface tension of the liquid (Vargha-Butler et al., 1994).

$$Cos\theta = \frac{\gamma_s - \gamma_{sl}}{\gamma} \qquad (2\text{-}3)$$

Contact angles of bitumen have been widely used, especially for surface tension calculations (Vargha-Butler et al., 1988 and 1994). Also, the contact angle is an important property in assessing wetting and adhesion of liquids to solids (Al-Maamari and Buckley, 2003).

The studies related to the contact angle of bitumen and asphaltenes can be separated in two distinct groups based on the phases present. The first group is contact angle measurements between oil and a solid in the presence of water, i.e. liquid-liquid-solid systems. Within this group are most of the studies performed under reservoir conditions. Examples of this type are the papers by Rao (2001) and Rao and Karyampudi (2002) who measured dynamic advancing and receding contact angles of crude oil under petroleum reservoir conditions (1-70 MPa and 25-200 °C). The findings were related to the interfacial adhesion and wettability of the asphaltenes and solid surfaces in a system involving vapor-liquid-liquid-solid phases.

The other group of measurements, more related to the present work, are when the contact angle of a liquid in contact with a solid surface is measured in a gas environment (gas-liquid-solid). Papirer and Fritschy (1981) measured the contact angle of bitumen modified with sulfur on mica in a nitrogen atmosphere at 94 and 138 °C using a goniometer. They found that the added sulfur improved the wettability of the bitumen on the mica surface by circa 5 °. Papirer et al. (1992) used also a goniometer to measure the contact angle between a water drop on an asphaltene surface (the measurements are assumed to be done in an air environment since no other comment was given in this regard). The asphaltene surface was prepared by evaporating the solvent from an asphaltene/toluene solution on a mica plate. Papirer et al. (1992) found poor wettability of the water on surfaces from three different asphaltenes, with angles between 86 – 95 °. Extensive measurements

were reported on the wetting and adhesion phenomena between tar (pitch) and coke material by Lahaye and Ehrburger (1985), who studied the pitch-coke interactions to estimate the ability of a molten pitch to penetrate a coke bed. To achieve their goal, they used transient contact angle as a means to measure the physicochemical properties of the interface and then calculate the change in the volume of molten pitch with time. Couderc et al. (1986) studied the effect of the temperature on the flow of a drop of pitch deposited on a bed of coke using the contact angle between the drop and the bed of coke as criteria of penetration or flow of the pitch into the coke. The measurements were done between 100 and 200 °C at a heating rate of 20 °C/h.

The standard method for measuring contact angle is to measure the geometry of the drop and determine the contact angle. Basu et al. (2004) presented an equation that allows for the calculation of the contact angle between a liquid drop and a solid surface using the spherical cap expression. The spherical cap expression assumes that the liquid drop is of the shape of the top part of a sphere sitting on a solid surface, as illustrated in Figure 2-2.

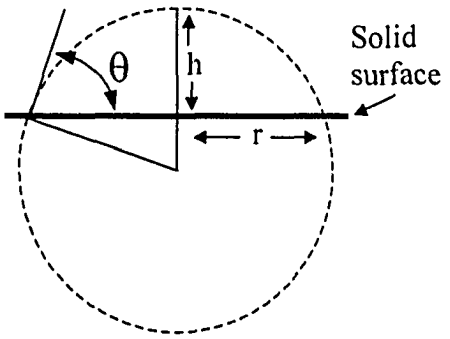

Figure 2-2. Schematic view of the cross section of a liquid drop on a solid surface

Equation 2-4 (Basu et al., 2004) relates the contact angle (θ) with the radius (r) and the height (h) of the liquid drop; it has been widely used for a range of liquids (Starostina et al., 2001; Basu et al., 2004). Equation 2-4 is also in agreement with other expressions proposed by Wu (1982) to measure the contact angle of melted or liquid polymer drops on solid surfaces. The only restriction for using this assumption would be the volume of the droplets. According to Wu (1982), the assumption works for small droplets of the order of 10^{-10} m^3.

$$Cos\theta = \frac{1-(h/r)^2}{1+(h/r)^2} \qquad (2\text{-}4)$$

The contact angle of liquid droplets on solids may vary with time. Once sitting on the surface, the liquid drop may spread on the surface until reaching its equilibrium position. The variation of the contact angle with time depends on the viscosity and surface tension of the liquid and also on the initial size (radius) of the liquid droplet (Bracke et al., 1989). In their work, Bracke et al. (1989) presented an expression for the relaxation time (τ_R) of the dynamic contact angle, assuming that the angle changes from 180 to 0° (complete wetting). In Equation 2-5, r_o is the initial radius of the liquid drop, μ is the viscosity, and γ is the surface tension of the liquid. Based in the Equation 2-5, it is clear that viscosity and surface tension are the predominant factors affecting the dynamics of the contact angle for droplets of an equivalent initial radius.

$$\tau_R = 4^{1/3}\frac{16\mu}{\gamma}r_o \qquad (2\text{-}5)$$

A better understanding of the wetting and adhesion characteristics of the asphaltenic material can be achieved studying their behavior as liquids without solvent. Unfortunately, such measurements have not been done.

2.4 LIQUID BRIDGE TECHNIQUE FOR MEASURING FLUID PROPERTIES OF HIGH TEMPERATURES REACTING SYSTEMS

In this section, the fundaments of an alternative technique to measure fluid properties at high temperature are presented. This technique allows for the measurements of fluid properties of reacting systems. At the same, not directly related with its fundamentals, the general arrangement of the apparatus makes it possible to visualize and video record the experiments for further analysis and verification.

2.4.1 THEORETICAL BASIS

The liquid bridge technique was originally proposed and successfully used by Gray et al. (2003) to measure the adhesive forces during the coking of AVR. In conjunction with an apparatus built for this purpose, they choose to measure the adhesives forces using this approach based on a number of criteria that included inert atmosphere, rapid heating, and the continuous removal of vapor products from the cracking reactions. By this technique, a liquid bridge is formed by touching and pulling apart two cylindrical rods each coated with a thin film of liquid. The

method is suitable for measuring properties at high temperatures with evolution of vapor products by reaction.

The model for measuring the adhesive forces was then taken by Aminu et al. (2004), who refined and complemented the model of Gray et al. (2003), making possible the measurement of the surface tension and viscosity from the same kind of experiments. To achieve this objective, Aminu et al. (2004) studied the surface and viscous forces involved in the formation, elongation and rupture of a liquid bridge between two cylindrical rods. They started from a model for a sphere and a plate for the surface force and used a dimensional analysis for developing an empirical solution for the viscous force. A simplified version of the geometry of the liquid bridge confirmed by Aminu (2003) by means of visual observation as well as mathematical calculations is shown in Figure 2-3. This figure shows all the variables from the liquid bridge require for the calculations.

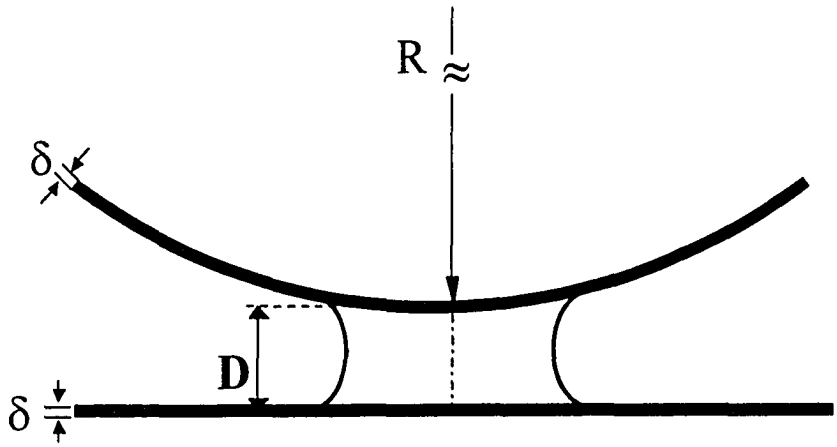

Figure 2-3. Cross section of a liquid bridge between to perpendicular crossing cylindrical rods. R is the radius of the rod, D is the distance between the rods, and d is the film thickness of the thin film coat

During the calibration experiments Aminu (2003) found that the viscous force was approximately equal to zero at the commencement of the formation of a liquid bridge. As a liquid bridge elongates to near its maximum elongation, the contribution of the surface forces became smaller and smaller and can be neglected in comparison to the viscous force. All the details and a more complete explanation of the derivation process of the set of equations were presented by Aminu (2003).

Because of the reacting regime, Aminu (2003) and Aminu et al. (2004) included a kinetic model as part of their set of equations. This kinetic model allows for the calculation of the film thickness (δ) of the thin film coat that surrounds both rods. This kinetic term is the only one that is a direct function of the reactive characteristics of the material under investigation.

2.4.2 MODEL

The final model for the measurement of the surface tension and viscosity using the liquid bridge technique can be summarized in a set of 3 equations.

When the liquid bridge is very short ($D \leq \delta$) then the force is mainly due to surface tension (Aminu, 2003):

$$F_T = 4\pi R\gamma \qquad (2\text{-}6)$$

Equation 2-6 relates the total force (F_T) measured with the surface tension (γ) of the sample, where R is the radius of the cylindrical rod. This measurement is made at the commencement of the formation of the liquid bridge.

As the bridge elongates, the total force is dominated by viscous forces. The relationship between the total force and the viscosity is shown in Equation 2-7.

$$F_T = 400\,\mu\frac{R^2}{D}\frac{dD}{dt}\left(\frac{\delta}{R}\right)^{0.752}\left(\frac{D}{R}\right)^{0.677} \qquad (2\text{-}7)$$

The new variables for in Equation 2-7 are the viscosity (μ), the film thickness (δ), and the distance between the rods or length of the liquid bridge (D). The term dD/dt is an independent variable that expresses the velocity at which the rods separate from each other, or at which the liquid bridge elongates. The empirical constants in Equation 2-7 were calculated by Aminu (2003) by using calibration oils of known properties.

The third equation, Equation 2-8, is specific for the kinetics of the thermal cracking of the AVR under certain conditions. This equation allows the calculation of the film thickness term (δ) required by Equation 2-7. This equation uses the initial film thickness ($\delta_{t=0}$) and two empirical parameters e_1 and e_2 to calculate the depleted film thickness at a given time of reaction (t).

$$\delta = \left[\delta_{t=0}^{(1-e_2)} + e_1 t\left(e_2 - 1\right)\right]^{\frac{1}{(1-e_2)}} \qquad (2\text{-}8)$$

As mentioned before, Equations 2-6 to 2-8 couple the measured forces with the actual fluid properties of the sample under investigation. Another very important part of the technique as a whole is the apparatus built by Gray et al.

(2003) for measuring adhesive forces, and later improved by Aminu et al. (2004) for the measuring of the surface tension. The configuration of the apparatus, with a closed housing allows the analysis of reacting samples. Its detailed description will be given in Section 3.3.1.

2.4.3 LIMITATIONS

The theoretical basis for the methods of Aminu et al. (2004) was developed on the basis of the formation of a liquid bridge between two surfaces. When the technique is applied to highly viscous petroleum or coke mixtures, the ability to form a liquid bridge becomes a limitation. The geometry of the bridge must be as close as possible to what Figure 2-2 shows. After being formed, the bridge also has to elongate to allow the application of Equation 2-7. On the other hand, an excessive elongation would allow temperature gradients within the bridge, because the bridge is heated indirectly, using rods of Curie-point alloy in an induction field. On the other hand, when the viscosity of the liquid is too low under the measurements conditions, the liquid bridge does not elongate enough to give readable measurement of its length and velocity of elongation before breaking, and the viscosity cannot be measured by this method. One more limitation about the liquid bridge is that it has to break in the middle, not just detaching from one of the rods. This uniform rupture would indicate that the liquid within the bridge was equally and completely wetting both surfaces. The flow regime along the liquid bridge is another concern, creeping flow for the liquid film flowing into a liquid

bridge has to be maintained to avoid any inertial or acceleration effects. For the range of film thickness and velocities used in this work, a Reynolds number < 2 was verified by Aminu et al. (2004).

All these limitations have to be taken into consideration when using the liquid bridge technique for measuring fluid properties. Visual verification of a proper formation, elongation and breakage of the liquid bridge should be included as a parallel and systematic procedure during all the experiments or measurements. By assuring that the mentioned stages of the liquid bridge are completed as expected, all the basic conditions would be fulfilled for the technique to deliver consistent results. In case of drastic changes of the experimental conditions, such as larger film thickness, or higher velocity of elongation of the liquid bridge, or lower viscosity, the Reynolds number would have to be verified to ensure operating in the creeping flow.

3. MATERIALS AND METHODS

In this chapter the materials and methods to conduct the experiments on measurement of fluid properties of AVR and asphaltenes are explained. The properties and characteristics of the feeds, chemicals, and other materials are presented first, the different devices used to measure the fluid properties are described, along with the procedures to prepare and conduct the experiments. Finally, some improvements made to the liquid bridge technique are explained.

3.1 FEEDS AND CHEMICALS

Four different feeds were used to carry out the studies. Syncrude Canada Ltd. supplied Athabasca vacuum residue (AVR) from Canada, consisting of the 524°C+ boiling fraction of the Athabasca bitumen. Idemitsu Kosan Inc supplied Maya VR from Mexico. Exxon-Mobil Research (New Jersey, U.S.A) supplied Arab Heavy VR from Saudi Arabia. The University of Petroleum (Beijing, China) supplied Gudao VR from China. Prepurified nitrogen was supplied by PRAXAIR Canada (Mississauga, Ontario, Canada). Solvents were from Fisher Scientific (Toronto, Ontario); all of them were used as supplied. The N62000 viscosity standard for viscometer calibration was supplied by Cannon Instrument Company (State College Pennsylvania, U.S.A.).

Toluene-insoluble solids were removed from AVR by dissolving 1 part of vacuum residue in 40 parts of toluene, sonicated for 30 minutes and then centrifuged for 30 minutes at a RCF of 25,000 gravities and 4 °C. The supernatant was recovered and the toluene was later evaporated by rotary evaporation. The rest of the vacuum residues had insignificant concentrations of solids; therefore, the solids removal step was omitted. Heptane (n-C_7) insoluble asphaltenes were separated using a solvent-to-vacuum residue ratio of 40 cm^3/g and mixing overnight. The asphaltene precipitate was recovered by filtration on a 0.22 μm Millipore filter at room temperature.

As pointed out by Alboudwarej et al. (2002), a number of factors can influence the yields of asphaltenes in laboratory separations. In industry practice, similarly, the composition of an asphalt fraction will depend on the exact operation of the deasphalting unit. Any changes to the separation method could alter the composition of the asphaltenes, and hence influence the fluid properties. In this study, therefore, we adopted the approach of separating the asphaltenes from different sources using a similar standard procedure, thereby allowing comparison of fluid properties on a common basis.

3.2 CURIE-POINT ALLOY RODS

The Curie-point is the temperature at which a material loses its magnetic properties. Nickel/iron (Ni/Fe) alloys have Curie-point temperatures that range from 160 °C to 1040 °C depending on composition. The rapid heating of the samples of AVR and asphaltenes in the laboratory was achieved by using Curie-point alloys in an RF induction furnace. The components of an induction furnace system are an alternating current (AC) power supply, an induction coil, and a work-piece (Curie-point alloy to be heated or treated). The power supply sends alternating current through the coil to generate a magnetic field. When the alloy is placed in the coil and enters the magnetic field, eddy currents are induced within the alloy, rapidly generating precise amounts of localized heat without any physical contact between the coil and the alloy. The temperature of the alloy rises until the Curie-point temperature is reached and magnetism is lost (Ameritherm Inc., Scottsville NY). The Curie-point alloys were used to fabricate the cylinders and flattened rods in the experimental apparatus in order to heat the samples to the desired temperature. The Curie-point alloy rods in conjunction with the induction furnace system provided safe, fast, and consistent heating.

The rods of Curie-point alloy used in this study for the surface tension and viscosity measurements came from four different sources. DyChrom (San Jose, California, U.S.A.) supplied the rod for temperatures of 312, 358 and 400 °C. These rods had diameters 0.62, 0.98, and 0.62 mm, respectively. The Curie-point alloy for temperature of 424 °C and 466 °C of diameter 1.63 mm and 1.47 mm,

respectively, were supplied by National Specialty Alloys (Houston Texas, U.S.A). AMETEK Specialty Metal Products Division (Wallingford, Connecticut, U.S.A) supplied the Curie-point alloy for temperature of 503 °C with a diameter of 1.96 mm. For temperature of 530 °C, welding rod (UTP Econocast 55NiFe-Cl, AIR LIQUIDE) was scraped of its flux and the rod turned on a lathe to a diameter of 2.04 mm. For the contact angle measurements, rods of 503 °C Curie-point alloy were modified to obtain a flat surface. Curie-point temperatures of the rods were verified by spot-welding 30-gauge type K thermocouple wire to the rod and measuring the temperatures in the induction field. The temperature profile was recorded using the BenchLink Data Logger (version 1.1, 1997) connected to a personal computer, and exported to Microsoft Excel for the analysis. All the Curie-point temperatures were measured in triplicate.

To maximize the coupling of the alloy with the induction field and to allow visual observation and video recording of the experiments, the rods were bent to a shape shown in Figure 3-1 for the surface tension and viscosity measurements and as shown in Figure 3-2 for the contact angle measurements. The rods had two opposing 45° bends, so that the ends of each rod were parallel to the axis of the induction coil. For the contact angle measurements, the rod was flattened in between the two bends, to provide a flat surface for measuring angle. The flattened section of the rods shown in Figure 3-2 was 9 mm long and 3 mm wide; the thickness of this section was 1 mm.

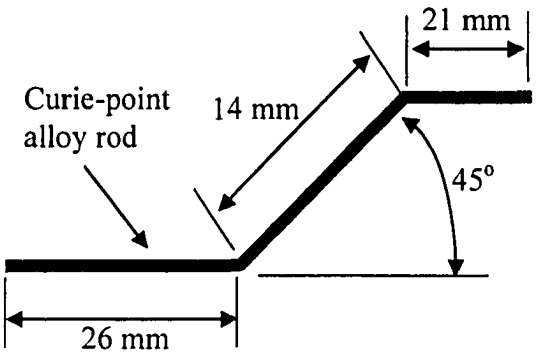

Figure 3-1. Shape of rod for surface tension and viscosity measurements

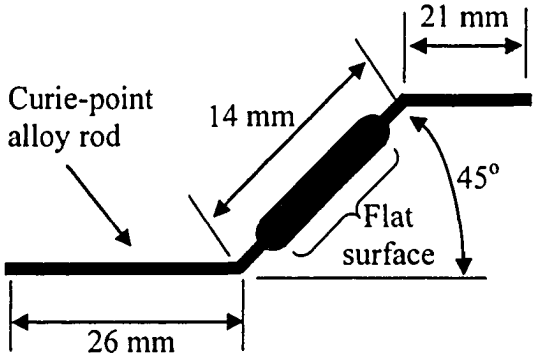

Figure 3-2. Shape of the rod for contact angle measurements

3.3 APPARATUS FOR MEASURING THE FLUID PROPERTIES

3.3.1 APPARATUS DESCRIPTION

A schematic of the equipment used is shown in Figure 3-3. Externally the equipment is a gas-tight acrylic box with a glass housing attached in one side. Each of the rods were mounted in a tube of Pyrex glass (diameter 3.9 mm), which was melted to hold the metal rods and then annealed to relieve stress. The Pyrex glass tubes were then attached to the hollow aluminum beams. As shown in Figure 3-3, one of the aluminum beams was connected, through a flexural pivot (spring pivot) model 5010-800 (Goodrich Rome, NY U.S.A.), to a linear variable differential transducer (LVDT1) model D540050HH (Daytronic Corporation, Dayton Ohio U.S.A.). The other aluminum beam and the plunger of LVDT2 were attached to a vertical motion stage, driven by a stepper motor model 5704M-0202 (The Motion Group Inc. Clovis CA U.S.A.). The two LVDT sensors were connected, through a signal conditioner model 3130 (Daytronic Corporation, Dayton Ohio U.S.A.), to a personal computer. The computer recorded data from the two LVDTs and controlled the stepper motor with the aid of the LabVIEW program (version 6.0, National Instruments Austin Texas U.S.A). An electric fan was mounted in the acrylic box to allow for mixing the nitrogen used as sweeping gas and the reaction vapor products, and speedy purging of air from the apparatus. All the equipment and parts were into the acrylic shell and the glass housing.

The glass housing of the equipment was placed inside of the coil of an induction furnace model XP-30 (Ameritherm Inc. NY U.S.A.) provided the heating

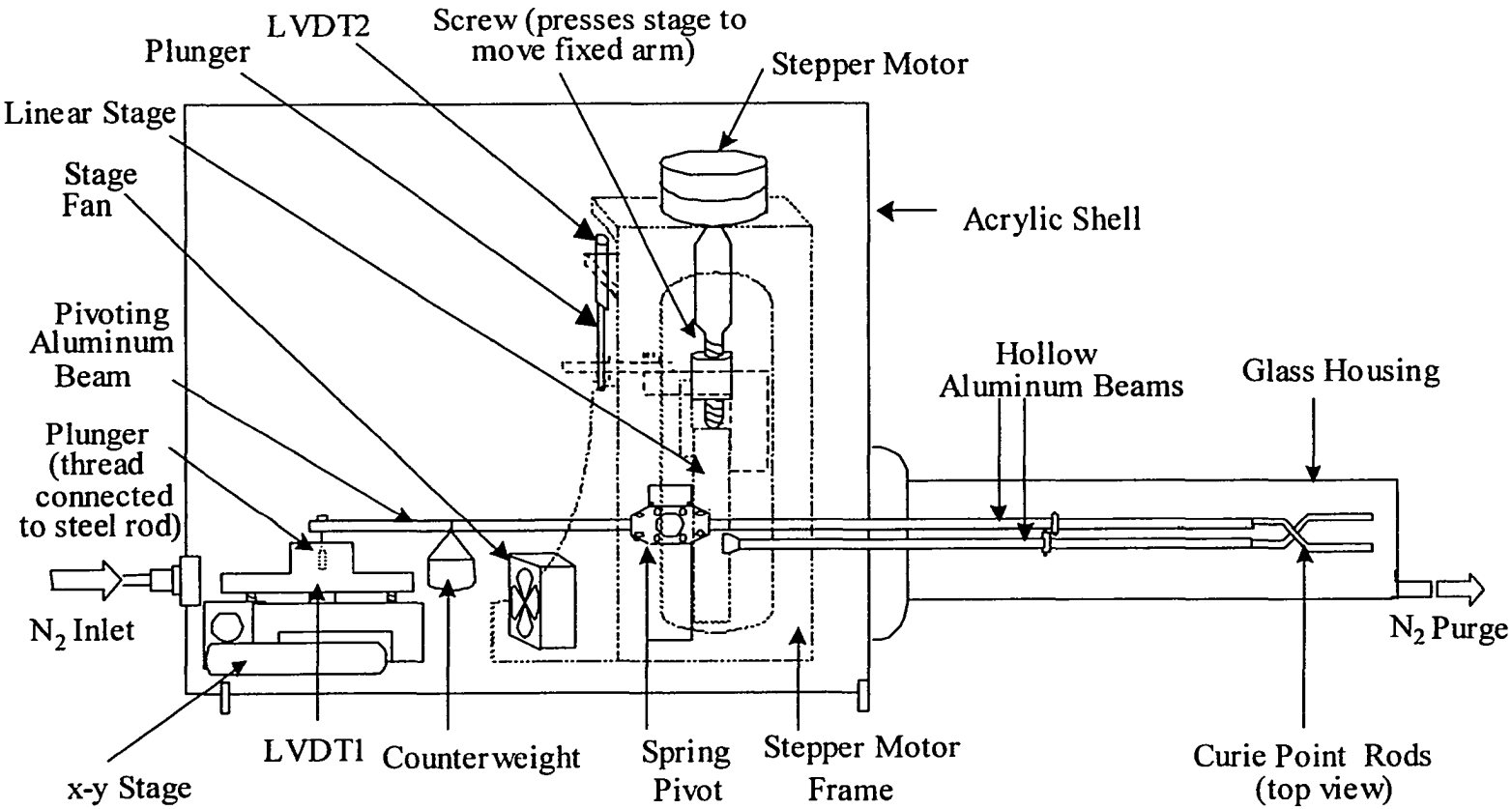

Figure 3-3. Schematic of the equipment for measuring the fluid properties

of the films of AVR and asphaltenes, by heating the Curie-point alloys. The heating coil of the induction furnace was connected to an induction furnace controller, which in turn was controlled by a personal computer. This personal computer also controlled the operation of the valve on the nitrogen line, all the controlling from this computer was done with the aid of the GeniDAQ program (version 3.11, Advantech Cincinnati OH, U.S.A).

3.3.2 Imaging Analysis Equipment

A video camera model TMC-7DSP (PULNiX America Inc., CA U.S.A.) and two high intensity filament lights model 3852582 and 4187531 (Lowel-Light Manufacturing Inc., NY U.S.A.) were focused on the samples. The video camera was connected to a television monitor model 20AF14C (Toshiba Inc., Ontario, Canada) via a video timer model VTG-33 (FOR.A Corp. Ltd., Japan) and a time-elapse VCR Super VHS model SVT-S480ES (Sony Corp., Japan). The trigger of the video timer was connected to the personal computer that hosted the LabView program. All the experiments were video taped using the VCR with Super VHS tapes. The elapsed time stamped by the video timer was used to determine the temperature at any moment based on the temperature profile of the specific rod used in a given experiment.

3.4 EXPERIMENTAL PROCEDURES

3.4.1 PREPARATION OF THE SAMPLES

Surface Tension and Viscosity

Each Curie-point rod with the attached glass rod was weighed on a balance. The unbent portions of the alloy were covered with masking tape, exposing only the centre portion, for the purpose of coating with solid-free AVR or asphaltenes. For the case of the rods to be sprayed with asphaltenes, a chemical etching was performed before the masking step to improve adhesion. For the chemical etching, the rods were submerged for 20 seconds in a solution of acetic acid, nitric acid, and acetone (1:1:1 v/v/v). A 2 wt % solution of the sample was prepared with methylene chloride and uniformly sprayed on the centre portion of the Curie-point rods. After spraying, the glass rod was cleaned and the coated rod was then left inside a fume hood for at least 48 hours to evaporate the solvent. Then, the masking tape was removed and the rod with the attached glass rod was weighed to determine the mass of thin film on the rod. The film thickness of the coat on the rod was calculated based on Equation 3-1, where m_{coated} is the mass in grams of the Curie-point rod-glass rod assembly after spraying, m_{dry} is the mass in grams of the assembly before spraying and taping, ρ is the density in kg/m^3 of the sample of interest (solid-free AVR or asphaltenes) and L is the length in cm of the sprayed portion of the alloy. δ and R are the film thickness in μm and radius in cm of the Curie-point rod, respectively. The taping, spraying and weighing process was repeated until attaining the desired film thickness.

$$\delta = \frac{m_{coated} - m_{dry}}{\rho (2\pi RL)} * 10^8 \qquad (3\text{-}1)$$

According to the results from Alboudwarej et al. (2002), the density of all the asphaltenes was assumed to be the same and equal to 1200 kg/m^3. More precise values of density are not required for the calculations. As it will be shown in Section 4.2.2 in a sensitivity analysis of the film thickness, this variable does not have a significant impact on the final results. As shown in Table 2-1, the density of the AVR was 1087 kg/m^3.

Contact Angle Measurements

For the contact angle measurements, flattened rods were used instead of cylindrical. Some flattened rods were coated with gold, aluminum, or coke. Some other measurements were done on the bare original Ni/Fe alloy. The coating of the metal was made using a Kurt J. Lesker sputter system. In the case of the gold coating, a previous coating of chromium was used to improve the adhesion of the gold on the surface. The thickness of the gold, aluminum, and coke coatings were approximately 150 nm (after 30 nm of chromium), 167 nm, and 1.5 μm; respectively.

To obtain a surface coated with coke, solid-free AVR was sprayed on the flattened part of the rod according to the procedure described above for the surface tension and viscosity. After the solvent evaporated, the rod was heated at ca. 500°C inside the induction furnace under a N_2 atmosphere for 120 seconds.

3.4.2 SURFACE TENSION AND VISCOSITY MEASUREMENTS

Two rods of the same Curie-point temperature coated with the same sample and with an equivalent film thickness, were inserted in the apparatus as shown in Figure 3-3. The two rods were positioned in such a way that they were both in a horizontal plane. The apparatus was then placed in the glass housing inside the induction furnace. The controlled rod (lower) was moved up with the stepper motor until it touched the free rod (upper), while making sure both rods stayed within the sensing range of the LVDT sensors. At this point, the two high intensity lights were switched on and the camera was focused at the touching point on the rods. The touching of the rods was verified visually and by reading the signal from the LVDT sensors. After verifying the touching point, the lights were switched off and the controlled rod was moved down by a predetermined number of steps. The time for the rods to touch was set at 15 seconds for all the experiments, so the samples were heated for the desired time while moving towards the touching point. The length of time the rods were pressed together was also set by a known number of steps, referred to as nudge amount. This nudge amount helped the formation of the liquid bridge, especially considering the highly viscous liquid in the same experiments. The moving of the controlled rod and the reading of the LVDT signals were done with the LabVIEW software. During the set up of the experiments, the software showed the motion of the lower rod and a digital visualization of the position of the two rods by means of the voltage signal from the LVTD sensors. During the actual

experiments, the software controlled the motion of the lower rod and recorded the voltage data with time (data acquisition) for further analysis.

For all the experimental runs, the apparatus was flushed with nitrogen for 20 minutes, initially at about 9 – 10 dm^3/min at 101.15 x 10^3 Pa, to rid the system of oxygen. The purge time was set in the GeniDAQ program that controlled the nitrogen flow and the start of the induction furnace. At 3 minutes before the end of purging, a session of LabVIEW was started for data acquisition and equipment control and the furnace power was switched on. The induction furnace controller was verified to be set at the maximum heating rate, which was ca. 60 °C/s in the case of the Curie-point alloy of 503 °C. This heating reach assured that 90 % of the Curie-point temperature was reached in 7 seconds. The temperature profile of the 503 °C Curie-point alloy rods is illustrated in Figure 3-4. About one minute before the end of the purging, the lights were switched on and the VCR was set to record. The nitrogen flow rate was changed and maintained during the experiments at about 1 dm^3/min. The reduction of the nitrogen flow allowed the stabilization of the upper (free) rod, and facilitated the subsequent calculation of the equilibrium voltage, which corresponded to the equilibrium position of the upper rod before being touched by the lower rod.

At the completion of purging, the GeniDAQ program switched the induction furnace on and started the timer, and using the LabVIEW the lower Curie-point rod was automatically moved until it touched the upper one. After the rods touched, they were pressed together by the nudge amount and afterwards

pulled apart by the motion of the controlled rod, which was moved down at a speed of 0.409 mm/s. This speed allowed the observation of bridge formation, elongation and rupture. After the formation of the liquid bridge between the rods, the free rod moved together with the controlled rod until a point when the liquid bridge was broken. Since the free rod worked on the principle of a microbalance, the adhesive force due to the liquid bridge would be sensed in terms of voltage by the LVDT1 on the other side of the pivot. The experiment was completed the moment the liquid bridge was broken. The lights, VCR, and furnace power were switched off and the data acquisition cancelled.

In addition to the data recorded, video recordings of the experiments with the stamped elapsed time were kept on videotape for further verification. The touching of the rods, possible dripping or excessive bubbling on the surface of the rods, and the liquid bridge formation, elongation and rupture were checked for each experiment. The data acquired from the experiments were then used to obtain values of viscosity and surface tension according to the procedure explained in Section 3.4.4.

3.4.3 CONTACT ANGLE MEASUREMENTS

Right before the experiments, the flattened rods were carefully cleaned with toluene, then with methylene chloride and air dried inside a fume hood. The rods were kept inside the fume hood for no longer than 1 hour, prior to being used for the contact angle measurements to avoid any deposit of dust on the rods.

One rod was inserted in the lower aluminum beam. The bent portion was positioned in a horizontal plane, then two or three particles of solid asphaltene were placed as shown in Figure 3-4a. The glass housing was connected and the equipment was set as illustrated in Figure 3-3 (without the upper rod). The apparatus was then displaced, placing the glass housing inside the induction furnace. At this point, the two high intensity lights were switched on and the camera was focused at the bent portion of the rod, where the solid asphaltene particles were located. After focusing the camera, the lights were switched off.

For all the experimental runs, the apparatus was flushed with nitrogen for 10 minutes at about 9 – 10 dm^3/min and 101.15 x 10^3 Pa to rid the system of oxygen. The purge time was set in the GeniDAQ program that controlled the nitrogen flow and the start of the induction furnace. At 2 minutes before the end of purging, the furnace power was switched on. The induction furnace controller was verified to be set at the minimum heating rate, which was ca. 10 °C/s in the case of the flattened Curie-point alloy of 455 °C. This heating rate gave a slow heating and hence facilitated the visualization of the melting process of the asphaltene samples. The temperature profile of the flattened rods is illustrated in Figure 3-5.

Figure 3-4. Melting of asphaltenes on a modified (flattened) rod for the contact angle measurements, a) before melting, b) molten asphaltenes

About one minute before the end of the purging the lights were switched on and the VCR was set to record. The flow of nitrogen was changed and maintained during the experiments at about 1 dm^3/min (same pressure). The nitrogen flow rate was reduced to avoid any possibility of convective cooling of the rod or samples by the flow of gas.

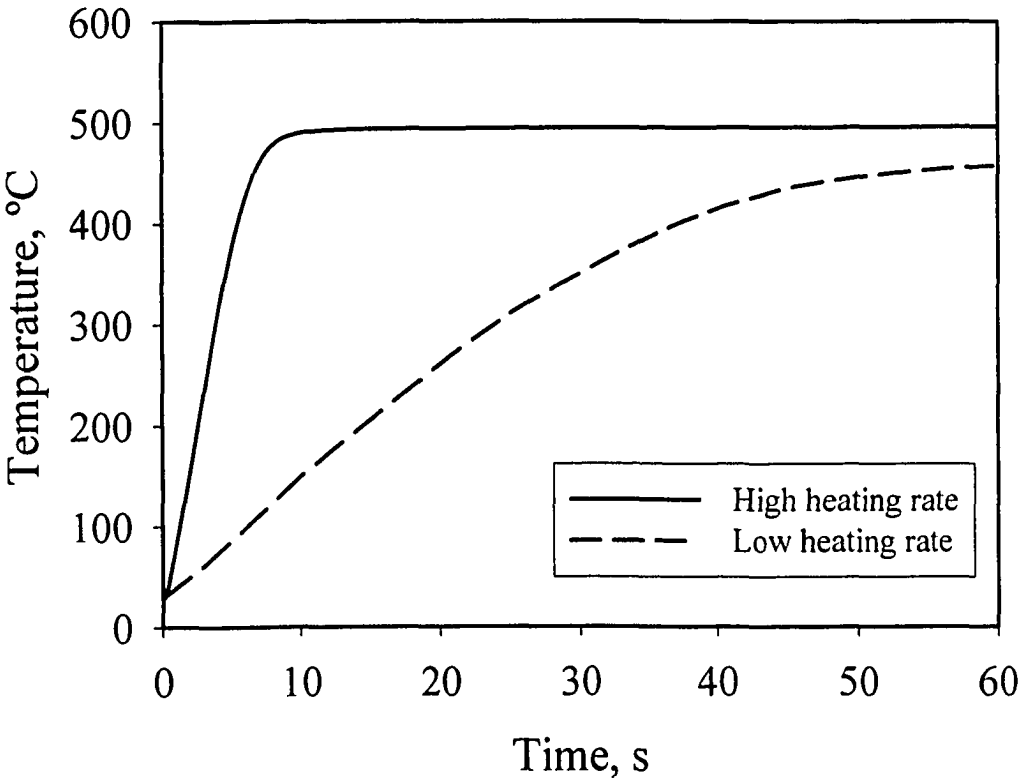

Figure 3-5. Temperature profile for Curie-point alloy rods at different heating rates. The solid line is for a rod of Curie-point temperature 503 °C, the dash line is for a flattened rod (Curie-point temperature 455 °C)

At the completion of purging, the GeniDAQ program switched the induction furnace on and started the timer. The melting process of the samples was observed in real time on the TV screen. The asphaltenes started losing the solid-like appearance and started melting as they were heated, flowing as a liquid or melt and finally adopted a classic liquid drop shape (Figure 3-4b). The total time of heating depended on the kind of measurements performed. For the dynamic contact angle, the heating of the samples continued until the onset of reactions, observed as bubbling of the liquid drops. For the equilibrium contact angle measurements, the samples were heated to 270 °C; after this point a temperature of 270 ± 5 °C was maintained for 180 seconds. Once the experiment was completed the lights, VCR, and furnace power were switched off. The temperatures during the experiments were verified and recorded by a HP Benchlink Data Logger connected to a spot-welded 30-gauge type K thermocouple wire located underneath the bent portion of the rod.

Video recordings of the experiments with the stamped elapsed time were kept on videotape for the calculation of the contact angle. The calculation procedure will be explained in the next section.

3.4.4 ANALYSIS OF THE DATA

Surface Tension and Viscosity

The data for the time course of the voltage from the experiments described in Section 3.4.2 were imported into Microsoft Excel. Voltage values from the two LVDT sensors were transformed into absolute position by means of Equations 3-2 and 3-3 (Aminu, 2003). Equations 3-2 and 3-3 relate the voltage (V) from the sensors LVDT1 and LVDT2, respectively, to the absolute position (h) of the upper (sub index u) and lower (sub index L) rods, respectively.

$$h_u = \frac{4.7598 - V_u}{4.6813} \tag{3-2}$$

$$h_L = \frac{7.6673 - V_L}{11.53} \tag{3-3}$$

$$F_T = 0.636 * (V_L - V_{eq}) - F_{mag} \tag{3-4}$$

As explained earlier, the force due to the liquid bridge acting on the upper rod was sensed in terms of voltage by LVDT1 on the other side of the pivot. The upper rod was free to rotate and worked on the principle of a microbalance. Hence,

the total force (F_T) acting on the upper rod was calculated based on the difference between the current (V_L) and the equilibrium (V_{eq}) voltages from the sensor LVDT1, with a correction for the magnetic effect of the induction field (F_{mag}) on the metallic rod (Aminu, 2003). The equilibrium voltage was calculated analyzing the time course of the data from the sensor LVDT1 in a graph, i.e. averaging the voltages reported by the LVDT1 when no force is acting on the free (upper) rod. The magnitude of the effect of the magnetic field effect was taken from Aminu (2003) and presented in Table 3-1. Equation 3-4 (from Aminu, 2003) was used to calculate the total force.

Table 3-1. Correction for Magnetic Effect of the Induction Field
(Aminu, 2003)

Curie-point Temperature, °C	Force Correction, mN
312	0.0053
358	0.0031
400	0.0065
424*	0.0084
466	0.0103
503	0.0144
530	0.0060

*Average value between 400 and 466 °C

Figure 3-6 schematically illustrates the time course of the absolute position of the two rods and the total force acting on the free rod. The time of commencement of formation of the liquid bridge, t_s, was determined applying a statistical test to the slopes of the two curves of absolute position of the rods (Aminu 2003). This test allowed detection of the time where the two rods started moving apart. From the time of the commencement of separation, and the data for the pull-off force, the force applied to the free rod at the commencement of the bridge elongation, F_S, was determined. The same procedure was repeated for the total force at the maximum elongation of the liquid bridge, F_V.

The surface tension and viscosity were then calculated using Equations 2-6 and 2-7. Equation 2-8 was used with the constants in Table 3-2 for measurement of viscosity of AVR at temperatures ≥ 400 °C, it was substituted with Equation 3-5 for the measurements of viscosity of asphaltenes and blends of AVR/AVR-asphaltenes at temperatures ≥ 400 °C. The process to obtain Equation 3-5 is explained in the Appendix A.

$$\delta = \delta_{t=0}[e_2 + (1 - e_2) * e^{-te_1}] \qquad (3\text{-}5)$$

Table 3-2. Kinetic parameters for depletion of film thickness of AVR, Equation 2-8 (Aminu, 2003)

Temperature, °C	e_1	e_2
400	$1.518.10^{-7}$	5.9841
466	$1.954.10^{-4}$	3.2128
503	$2.444.10^{-3}$	2.6618
530	$3.770.10^{-3}$	2.7340

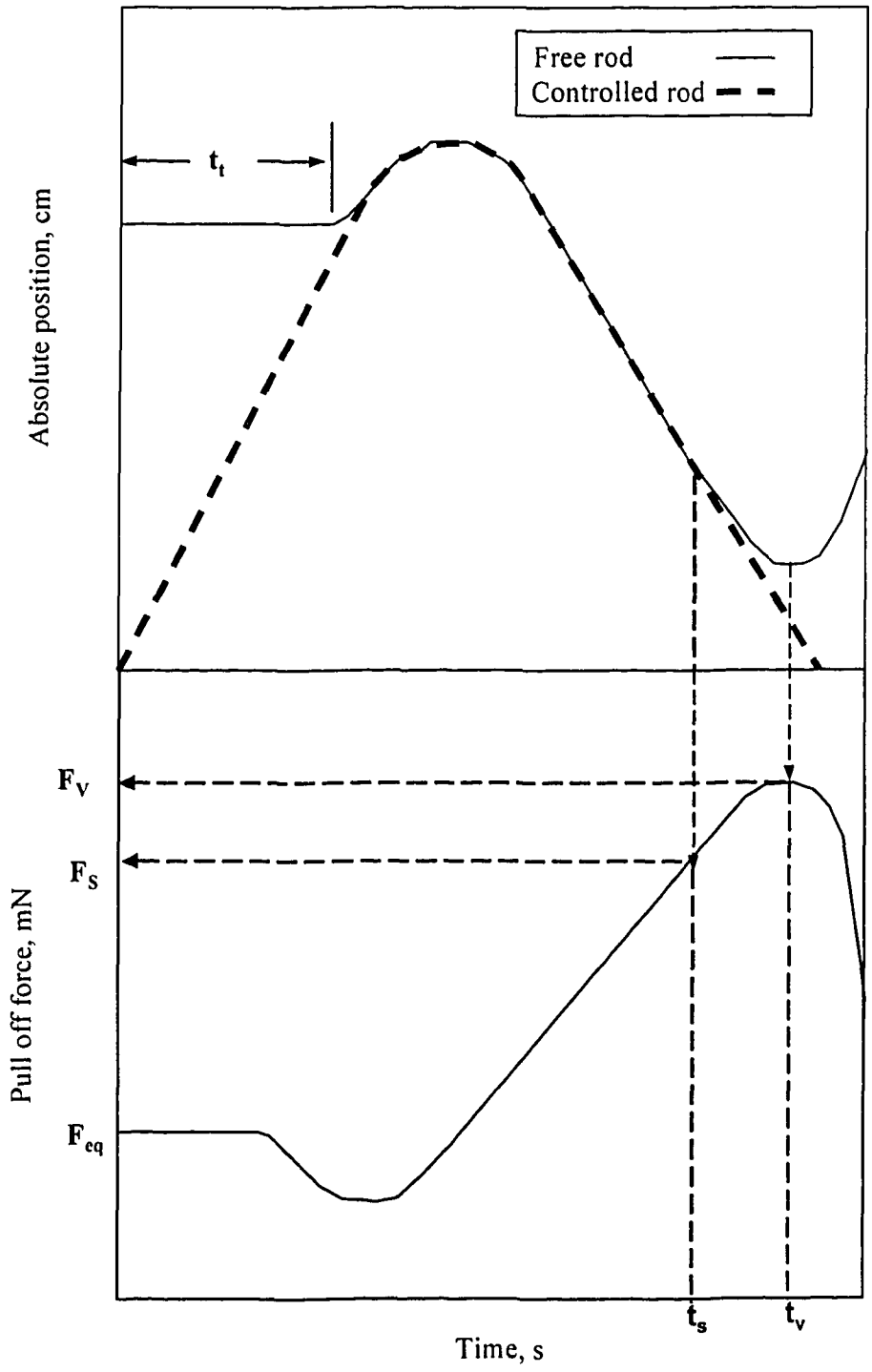

Figure 3-6. Typical time course of an experiment of measurement of surface tension and viscosity. t_t is the heating time to touch the rods, t_S is the heating time at the commencement of the bridge elongation, t_V is the heating time at the maximum elongation of the liquid bridge, F_S and F_V are the force at t_S and t_V, respectively. F_{eq} is the force at equilibrium before the touching, it is equal to zero (not shown for clarity)

Contact Angle

The video recordings of the experiments described in Section 3.4.3 were used to observe the melting of the asphaltene samples and to calculate the contact angle between the liquid drops and the solid surfaces. Melting of the asphaltenes, or at least partially melting, was responsible for the observed behavior because no volatile compounds were present in the asphaltene samples (Gray et al., 2004a). The asphaltenes only started to lose mass once they reached the temperature where the cracking reactions started to take place (ca. 400 °C). The video was played in the VCR and visualized on the TV; once the desired image was observed on the TV screen the video was paused. The required measurements for the contact angle calculation were taken from directly from the enlarged image on the TV screen. This procedure of taking measurements from magnified images on a TV screen to calculate the contact angle of a gas-liquid-solid interphase was successfully used by Debacher and Ottewill (1991). They compared the results using the TV images to microscopy and found very good agreement in the results.

Equation 2-4 was used to calculate the contact angles from the data of the drop radius and heights from the magnified images in the TV screen. In the case of the dynamic contact angle calculations, the video was paused right after the apparent complete melting of the asphaltenes. The temperature for the complete melting ranged between 190 and 250 °C. The temperature shown by the thermocouple was assumed to be the same as the surface in contact with the asphaltene samples, because the heat transfer resistance due to the thin coatings of

gold, aluminum and coke was neglected. The observed temperatures for the melting of the asphaltenes were very close to the results of Gray et al. (2004a) shown in Table 2-4. The differences could be due to the differences in the technique, heating surface area and material, and statistical variation, given the error bars in their work.

For the equilibrium contact angle calculations, the video was paused several times after 90 seconds of heating, and several contact angles were calculated using Equation 2-4, until the value did not change any more within the experimental error. Constant contact angles were always observed after 120 seconds of heating.

3.5 IMPROVEMENTS TO THE LIQUID BRIDGE METHOD

3.5.1 EXTENSION OF THE CALIBRATION RANGE OF VISCOSITIES

Aminu (2003) developed the liquid bridge technique based on calibration oils of up to 22 Pa.s. His results for viscosity of AVR, exceeded this value of 22 Pa.s several times. For this reason, and to allow for higher viscosity asphaltenes, the liquid bridge technique was tested with a more viscous calibration oil. Several experiments were performed at room temperature using the N62000 silicone oil, with a viscosity of 200 Pa.s at room temperature. The oil was sprayed as described in Section 3.4.1 on 1.96 mm rods. After the experiments at room temperature, the data was analyzed as described in Section 3.4.4. The results of this new calibration, together with the results from the calibration from Aminu (2003) are shown in Figure 3-7. The range of the correlation for the viscous force was then expanded to viscosities up to 200 Pa.s.

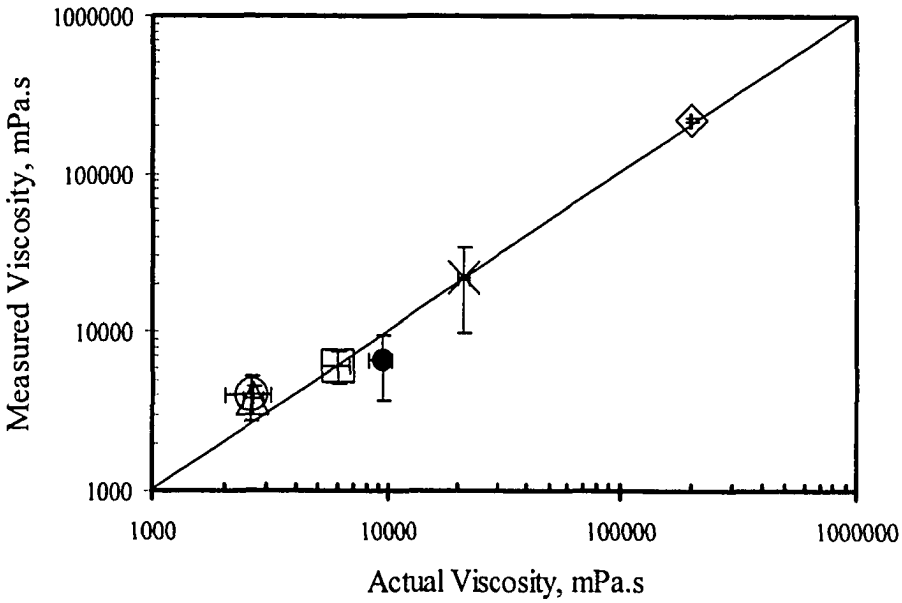

Figure 3-7. Extension of the calibration of the equipment
(values below 10^5 mPa.s from Aminu, 2003)

3.5.2 SIGNAL NOISE REDUCTION

Another improved feature of the operation of the apparatus for the liquid bridge method was the filtering of the voltage data from the LVDT sensors. The original data obtained by Aminu (2003) contained significant high-frequency RF noise from the field of the induction furnace acting on the LVDT sensors of the equipment. Consequently, Aminu (2003) filtered the data using software previous to any other analysis. In this work, special attention was paid to removing the noise and avoiding the used of the digital filtering. A considerable improvement of the original signal was achieved by changing the AC power supply of all the electronic devices to a separate power network, separate from the high voltage AC network

used to feed the induction furnace. The electronic parts were also moved as far as practically possible from the induction coil. A comparison between the original voltage signals (from the LVDT1) before and after the improvements is shown in Figure 3-8. After the improvements, the digital filter was no longer required for the analysis of the voltage data.

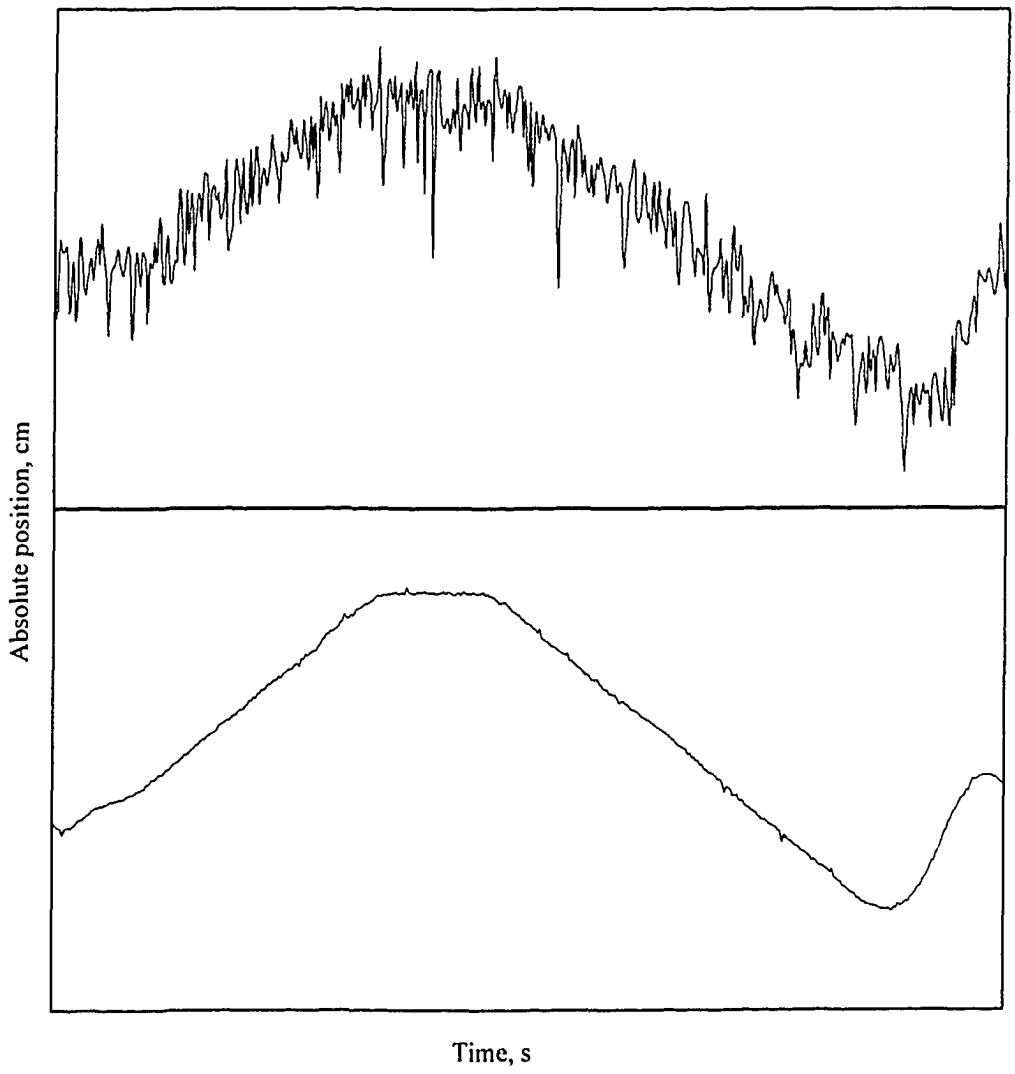

Figure 3-8. Improvement of the signal from the LVDT1
(lower-controlled rod position not shown for clarity)

4. RESULTS AND DISCUSSION

In this chapter the results for the fluid properties are presented and discussed. The first property presented is surface tension, then the viscosity, followed by the contact angle results. The effect of the bitumen solids on the fluid properties is discussed later, and finally comments on the process implications of the findings of this research are provided. All the results are shown as graphs of property versus temperature or property versus composition. In both cases the error bars show the standard deviation calculated from the experimental runs, which were completed at least in triplicate.

The three fluid properties under investigation in this work were measured for asphaltenes separated as described in Section 3.1, isolated from four different vacuum residues; Athabasca, Maya, Arab Heavy, and Gudao. These sources were selected as representation of asphaltenes from completely different geological formations around the world. These asphaltenes span a range of sulfur and nitrogen contents, as well as a range of aromatic carbon content (Rahmani, 2003a).

When working with vacuum residues and asphaltenes at high temperatures, some special considerations regarding the composition of the samples have to be taken into account. According to Zuo and Lui (1994) and Gray et al. (2004b), at temperatures beyond 400 °C vacuum residues and asphaltenes start reacting (cracking and devolatilization). For this reason, different temperatures were used during the measurements of the fluid properties. The ranges of temperature were selected depending on the sample under measurement, the properties of the material

under analysis, and the applicability of the results. For the surface tension and the viscosity the main range was between 312 and 530 °C. Within this range 7 different temperatures were selected, i.e. 312, 358, 400, 424, 466, 503, and 530 °C. Other ranges or temperatures were also used such as 312 – 358 °C for non-reacting regime measurements, and a fixed temperature of 503 °C for studying compositional effects. For the contact angle measurements the temperature was not fixed, but instead was determined by the melting behavior of the asphaltenes under analysis.

4.1 SURFACE TENSION

The surface tension of asphaltenes, AVR, and blends of AVR/AVR-asphaltenes was measured by means of the liquid bridge technique, as described in Section 3.4. In this section the results for the AVR-asphaltenes are presented first, then the results for other asphaltenes and later the effect of the asphaltene content are presented.

4.1.1 SURFACE TENSION OF ASPHALTENES

For the AVR-asphaltenes the surface tension was measured at 7 different temperatures, from 312 to 530 °C. The results are shown in Figure 4-1.

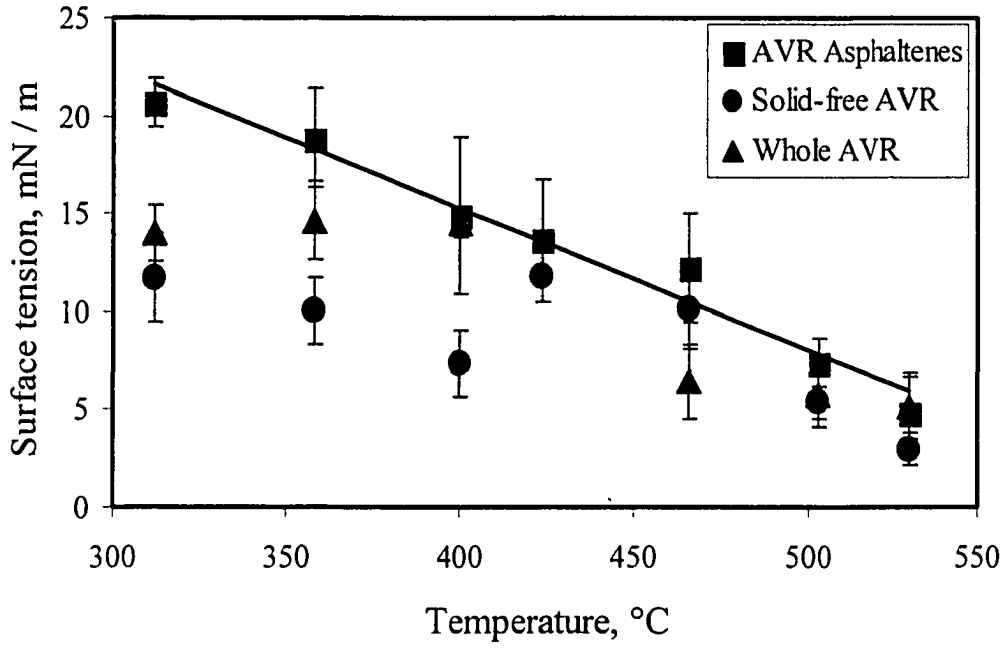

Figure 4-1. Surface tension of Athabasca VR asphaltenes versus temperature, t_t = 15s. The solid line is from the linear regression of the data points for AVR Asphaltenes. Data for whole AVR from Aminu (2003)

Before commenting about these results or making any comparison with other work, an important issue must be addressed; the composition of the sample at the moment of the measurements. The data presented here do not reflect the surface tension of the original AVR-asphaltenes beyond 400 °C, due to thermal reactions. However, according to Aminu (2003) the surface tension of hydrocarbon mixtures is not affected by composition, within the experimental error.

In the range of temperatures illustrated in Figure 4-1 the surface tension of the AVR-asphaltenes decreases from 20.7 at 312 °C to 4.8 mN/m at 530 °C. This decrease of the surface tension seems to be monotonic, and no evidence of any significant disruption was found. Aminu (2003) and Aminu et al. (2004) measured

the surface tension of AVR in the range of temperatures 312 – 530 °C, they found that the surface tension decreased from ca. 14.7 to 5.1 mN/m, but not in a monotonic way. The results from Figure 4-1 show that the surface tension of the AVR-asphaltenes was higher than the surface tension of the AVR in the lower temperature regime (< 400 °C). Above 400 °C there was no significant difference between the surface tension values. The results at lower temperature agree with the comments from Wu (1982) and Potocnzy (1984). Working under non-reacting conditions, they stated that the surface tension increases with the molecular size. In the high temperature regime, reactions made the two materials similar.

The data from Figure 4-1 show that the surface tension of the AVR-asphaltenes decreases with temperature as expected. A linear regression of these data is shown also in Figure 4-1, and the equation for this regression is shown in Equation 4-1.

$$\gamma_{AVR-asph} = -0.072\,T + 43.96 \qquad (4\text{-}1)$$

The decrease of the surface tension with temperature has been seen experimentally for crude oils and bitumens, by Da Silva Ramos et al. (2001) between 5 and 45 °C, and by Isaacs and Smolek (1983) between 50 and 150 °C. According to Wu (1982), similar trends are observed for liquid or melted polymers. Aminu (2003) and Aminu et al. (2004) also observed the same trend for AVR between 312 and 530 °C, however, they did not see a consistent monotonic decrease trend likely due to the larger uncertainty of their measurements due to the signal noise and digital filtering.

The surface tensions obtained by the liquid bridge technique for temperatures above 400 °C are dynamic measurements, because the composition of the liquid and the gas at the interface were not in equilibrium. The liquid phase was undergoing cracking and the light products of the reactions passed to the gas phase and were swept away by the continuous flow of nitrogen.

With the aim of investigating whether or not the surface tensions of the AVR-asphaltenes were typical for petroleum asphaltenes, the surface tension of other asphaltenes were also measured. The results are illustrated in Figure 4-2. These measurements were performed in a lower range of temperatures to avoid the reacting regime.

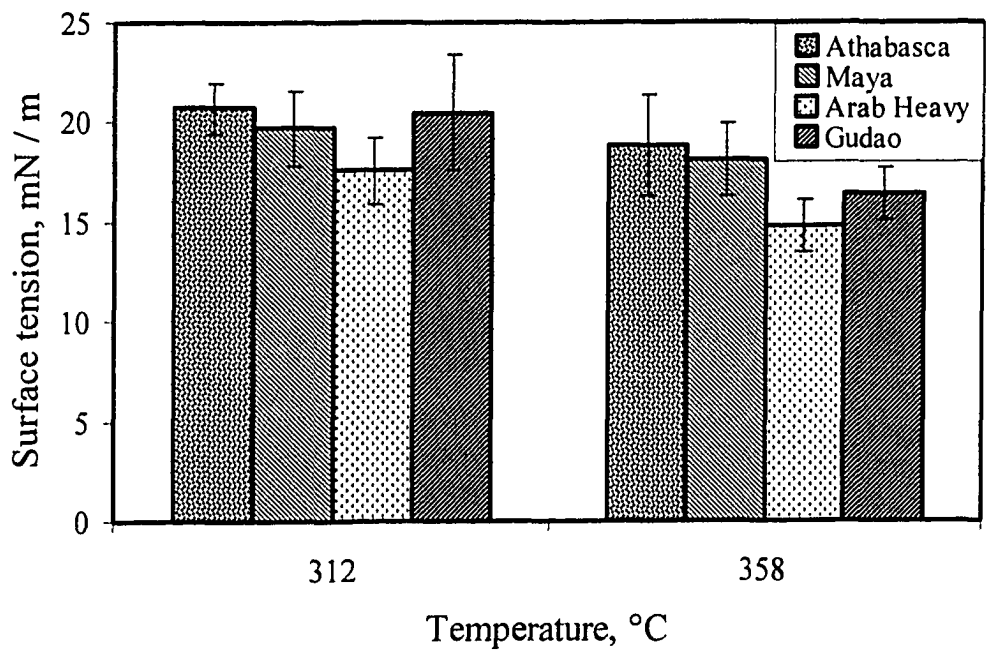

Figure 4-2. Surface tension of asphaltenes at low temperature (t_t = 15s)

The data of Figure 4-2 show that the surface tension of the AVR-asphaltenes was not unique, but was a typical result for *n*-heptane asphaltenes at these temperatures and under these conditions. The expected decrease of the surface tension as the temperature increases was also observed for the other samples. At 312 °C, the average values of surface tensions differed by only ca. 3 mN/m and at 358 °C by ca. 4 mN/m. The surface tensions for all the asphaltenes at 312 and 358 °C were greater than the corresponding values of surface tension for the AVR (Aminu et al., 2004).

Statistically (to 95 % confidence), the only asphaltene whose surface tension differed from the rest was Arab Heavy. Its surface tension at 312 °C (17.6 mN/m) was statistically lower than the surface tension of the Athabasca VR asphaltenes (20.7 mN/m), and at 358 °C (14.8 mN/m) it was lower than surface tension of asphaltenes from Athabasca VR (18.8 mN/m) and Maya VR (18.2 mN/m). This small difference was not correlated with any chemical or structural characteristic of the Arab Heavy VR or its asphaltenes.

4.1.2 Surface Tension of Blends of AVR/AVR-Asphaltenes

Several blends of AVR with AVR-asphaltenes were prepared. The samples differed in the weight fraction of asphaltenes, ranging from 0 % (i.e. maltenes only) to 100 %. The original solid-free AVR was taken as a blend with circa 30 wt % of asphaltenes (see Table 2-1), and the AVR-asphaltenes (Section 4.1.1) at 503 °C were taken as a sample containing 100 wt % of asphaltenes. All these measurements were done for experimental simplicity at 503 °C. With these

measurements the properties of the reacting mixture were calculated. The results are shown in Figure 4-3.

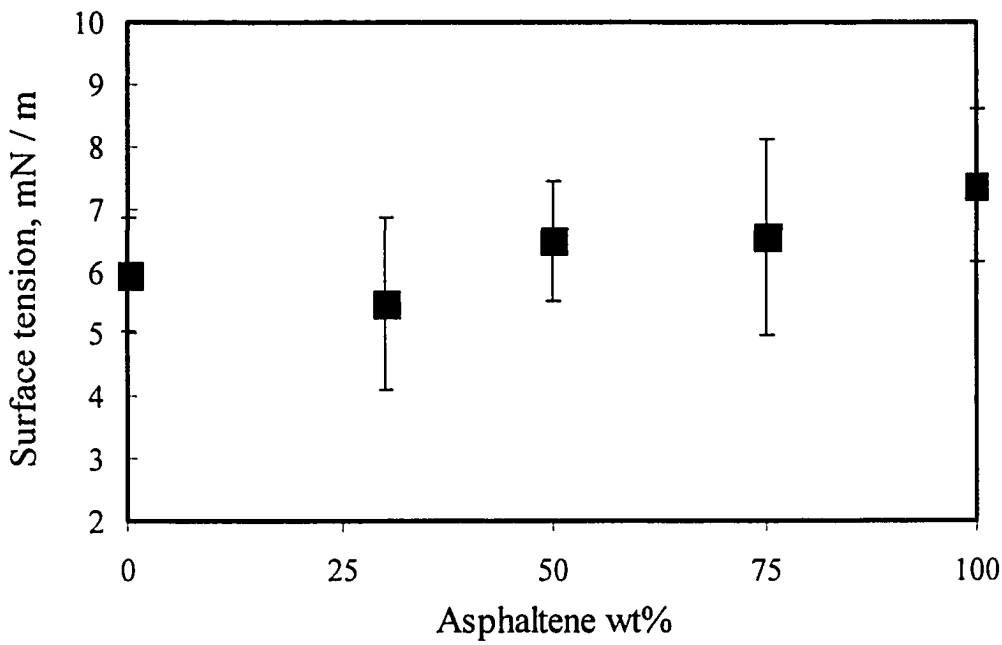

Figure 4-3. Surface tension of Athabasca VR/Athabasca VR asphaltene blends versus weight percent of asphaltene at 503 °C (t_t = 15s). The x-axis indicates the initial composition of the blend (t = 0)

Although the data in Figure 4-3 might seem to indicate an increase in the surface tension with the initial asphaltene weight fraction (at t = 0), statistically (95 % of confidence) there was no change in the surface tension with the initial asphaltene content. The slope of the linear regression was 0.02 ± 0.04; therefore, the surface tension can be taken as a constant for practical purposes, regardless of the initial amount of asphaltene at the beginning of the measurement. Given the importance of this finding, it is noteworthy to clearly state a key feature of Figure 4-3. Due to thermal reactions, the composition of the sample at the time of

measurements will not be the same as at the beginning of the experiment. Hence, the x-axis of Figure 4-3 does not necessarily indicate the actual composition of the samples for the corresponding surface tension values.

The average surface tension from Figure 4-3 was 6.37 mN/m with a standard deviation of 1.26 mN/m (n = 21). These results are in agreement with the findings from Aminu (2003), who observed that the surface tension was insensitive to the changes in composition due to reaction at a given temperature. Drelich et al. (1994) also claimed no relationship between the composition of the bitumen and its surface tension. For dilute mixtures of asphaltenes in organic solvents at much lower temperatures, the results for surface tension of asphaltenes found in the literature are in general agreement. According to Sheu et al. (1992), Rogel et al. (2000), and Da Silva Ramos et al. (2001) the surface tension of these dilute mixtures decreased with increasing fraction of asphaltenes, due to the role of the asphaltenes as surfactants at the liquid-gas interface. At elevated temperatures, as illustrated in Figure 4-3, such surfactant properties were not observed.

4.2 VISCOSITY

The viscosity of asphaltenes, AVR, and blends of AVR/AVR-asphaltenes was also measured by means of the liquid bridge technique. The viscosity results were obtained from the same experiments that gave the surface tension results (previous section). In general, the aim of the viscosity measurements was to

determine the role of composition, but the influence of temperature and extent of reaction on the viscosity was also studied.

The only published data for viscosity of bitumen, vacuum residues and asphaltenes at temperatures above 300 °C are from Aminu (2003) and Aminu et al. (2004). Hence, all the comparisons within this section are made with these viscosities of AVR at temperatures from 180 to 530 °C.

4.2.1 Viscosity of Asphaltenes

The data of Figure 4-4 show the results of viscosity measurements for AVR-asphaltenes. The analysis of this figure will be separated in two well-defined regimes. The first is a non-reacting regime, 312 – 400 °C. The other is a reacting regime, above 400 °C.

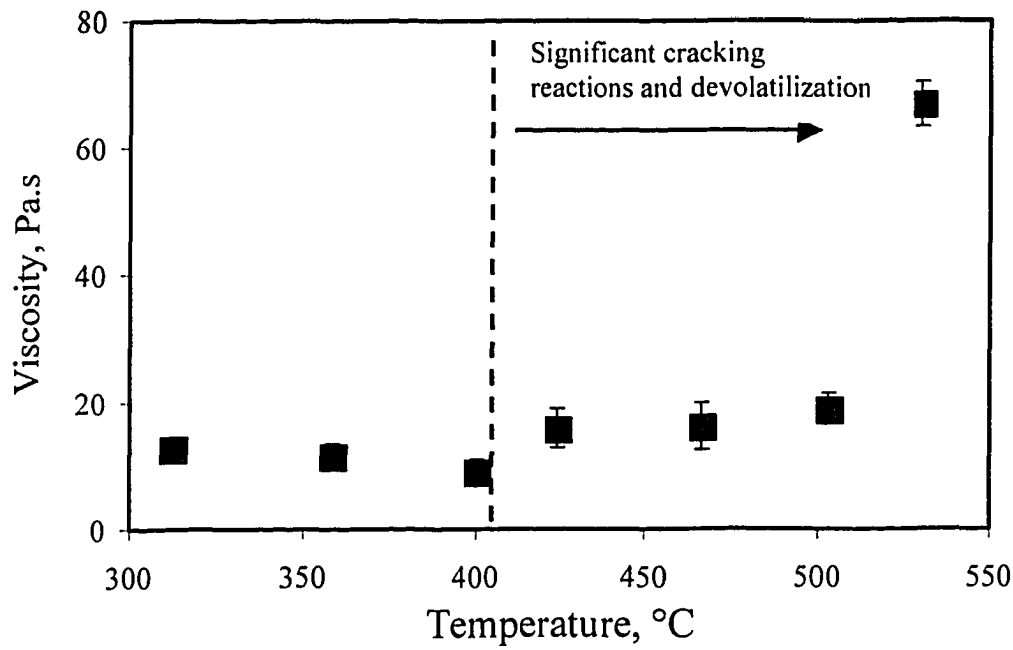

Figure 4-4. Viscosity of AVR-asphaltenes versus temperature, t_t = 15s

AVR Asphaltenes in the Non-Reacting Regime

For clarity, the results for the non-reacting regime are shown along with other results in a separate figure (Figure 4-5). Constant composition was assumed in this regime, because no significant cracking reactions would be expected to occur below 400 °C during the measurements. Figure 4-5 shows that the viscosity decreased with temperature, from 12.8 Pa.s at 312 °C to 9.3 Pa.s at 400 °C (about 3.5 Pa.s), giving a slope of – 0.039 Pa.s/°C.

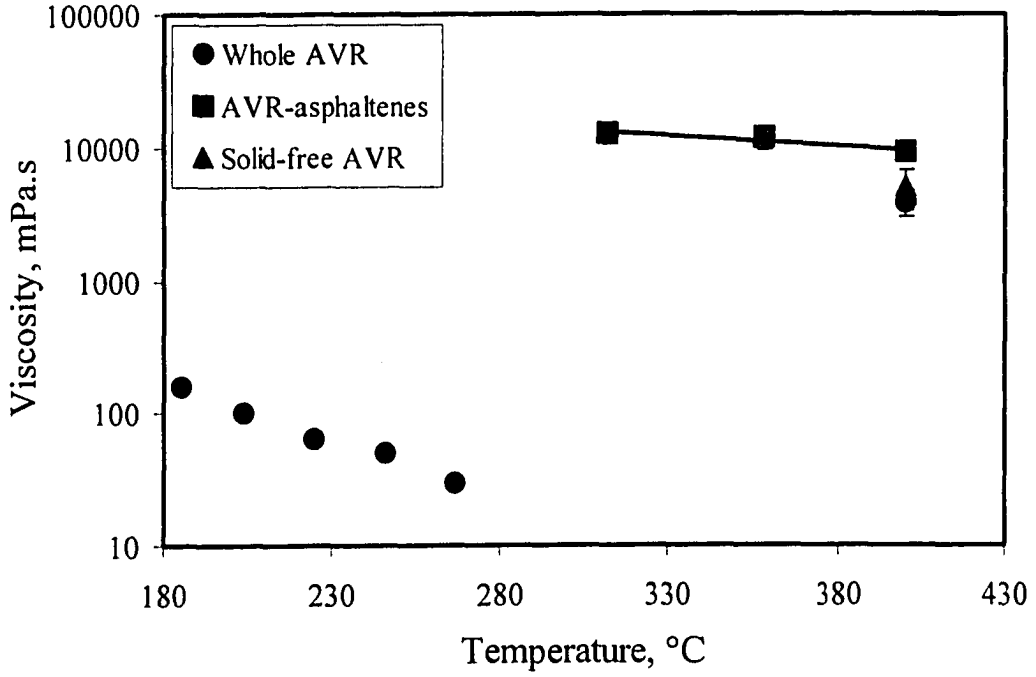

Figure 4-5. Viscosity of Athabasca VR and Athabasca VR asphaltenes in the non-reacting regime. Data between 180 – 300 °C from RMS, above 300 °C from liquid bridge technique (t_t circa 15s). Data for whole AVR are from Aminu (2003). The line is from the linear regression of the data asphaltenes data points

The trend shown in Figure 4-5 for the viscosity in the non-reacting regime was expected, following the well-known effect of the temperature on the viscosity of liquids such as bitumen and its fractions (Mehrotra, 1992). For the case of bitumen and vacuum residues, several models have been proposed to fit viscosity versus temperature data (Mehrotra et al., 1996), but no information is available in the literature for the trend of viscosity with temperature at such high temperatures, i.e. above 300 °C. However, the data for the viscosity of the AVR-asphaltenes versus temperature was successfully fitted within the experimental error with the Walther double logarithmic equation (Mehrotra 1990). The linear regression is shown in Figure 4-5 as a solid line. Figure 4-5 also shows that the viscosity of the AVR-asphaltenes is higher than the viscosity of AVR (whole and solid-free) at 400 °C, but within the same order of magnitude.

Figure 4-5 also shows the viscosity of the whole AVR at lower temperatures (180 – 300 °C) obtained from a Rheometric Mechanical Spectrometer (Aminu, 2003). At lower temperatures, around 300 °C, the difference between the viscosity of the whole AVR and AVR-asphaltenes was greater than at 400 °C. An extrapolated value of viscosity at 312 °C for the AVR, from the RMS data, was about 3 orders of magnitude lower than the corresponding viscosity for AVR-asphaltenes, i.e. of order 10 mPa.s versus 10^4 mPa.s. Data for AVR below 400 °C are not presented because of the low adhesive forces showed by this material at such temperatures, i.e. 312 – 358 °C. At 400 °C the volatilization of light components from the AVR was likely be significant, affecting the viscosity.

Because of this volatilization, the viscosity of the AVR samples apparently increased to a point where it was possible to measure the adhesive forces with the liquid bridge apparatus. Loss of volatiles during measurements is the only possible explanation for the difference between the viscosity measured for AVR below 280 °C, and the measurements at 400 °C. The data at 312 °C indicated that the molten asphaltenes were 3 orders of magnitude more viscous than the extrapolated estimate for the intact blend of maltenes and asphaltenes in the original vacuum residue.

AVR Asphaltenes in the Reacting Regime

The results for the regime above 400 °C are shown in Figure 4-6. At these high temperatures (424 – 530 °C) the composition of the sample was changing constantly. The heating time at which the rods touch (t_t) was the same value of 15 seconds for all the temperatures, within the experimental error. The time at which the viscosity was measured (t_v) was not controlled, therefore it was not strictly the same between samples. Due to the dependence of reaction on temperature, the composition of the samples was not be the same for the different temperatures at a given time of measurement. Based on the findings of Rahmani et al. (2002) and other considerations, a first order kinetic model was used to estimate the film thickness of the AVR-asphaltenes at any given time for a specific temperature. The development of the model is explained in the Appendix B, its final expression is Equation 3-5. From this kinetic model, the higher the temperature the faster the

advance of the cracking reactions, i.e. a larger extent of reaction for the same heating time. Hence, the results shown in Figures 4-4 and 4-6 must be treated carefully. Above 400 °C the measured viscosities are for material of a different composition, and possibly even at 400 °C for AVR due to loss of volatile components.

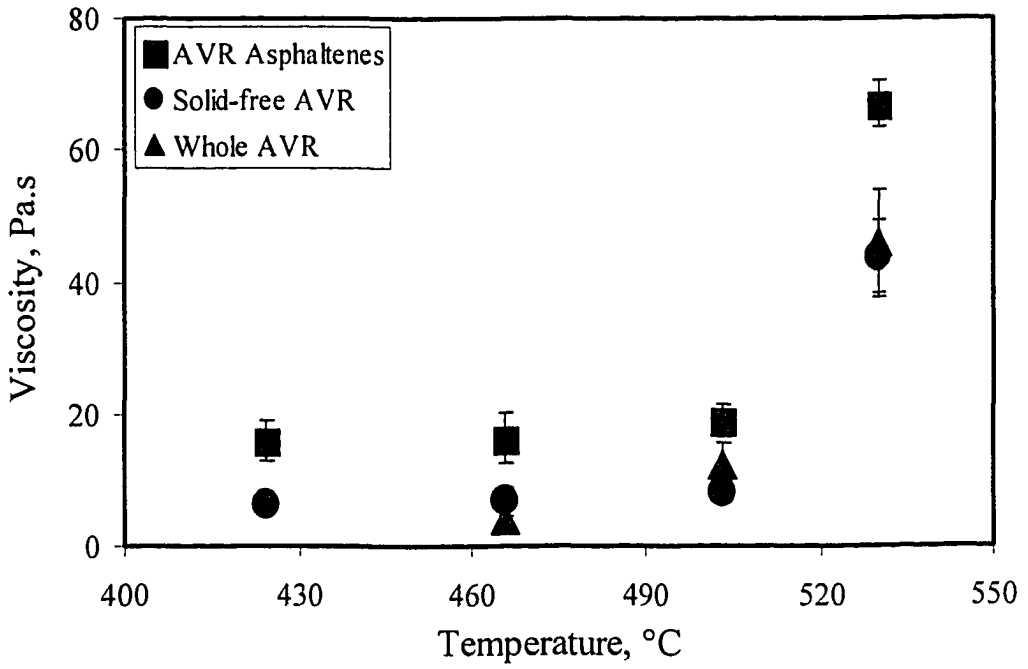

Figure 4-6. Viscosity of Athabasca VR and Athabasca VR asphaltenes at the reacting regime, t_t = 15s. Data for whole AVR from Aminu (2003)

Although composition was variable in the reacting regime (Figures 4-4 and 4-6), the increase in viscosity with temperature was real. The reason for this increase in viscosity was compositional change. As the temperature increased,

cracking reactions occurred faster, thus the remaining material at the time of measurement was heavier and heavier. In other words, what was still on the rods at t_v seconds of reaction at 466 °C consisted of much lighter components than what was still present at the same time at 530 °C. Kinetics of cracking and devolatilization of vacuum residues under similar conditions were studied by Gray et al. (2004b). A reduction of circa 80 % of the extract fraction (weight fraction of feed) was observed by raising the temperature of reaction from 457 to 530 °C for a 15 seconds cracking reaction. A consistent effect of the temperature on the viscosity is observed in Figure 4-6. The viscosity did not increase significantly between 424 and 466 °C, but it did change dramatically from 466 to 530 °C. As a consequence of the important compositional effect on the viscosity at these temperatures, no attempt was made to fit these data into a viscosity-temperature correlation. Comparison of the viscosity of the AVR-asphaltenes with the AVR (Figure 4-6) shows that the asphaltenes were a more viscous material in the temperature range between 424 – 530 °C. The results were within the same order of magnitude, but the viscosity of the AVR-asphaltenes was of at least 2 times the viscosity of the AVR in this temperature range.

Other asphaltenes

The viscosity of the AVR-asphaltenes was compared with results from other asphaltenes in a similar fashion to the surface tension, in the non-reacting regime. For the other asphaltenes, data were not available to calculate the extent of reaction and the film thickness above 400 °C. Hence, lower temperatures (312 and 358 °C) were used to avoid the reaction regime and measure the fluid properties without any further assumption. The results of the measurements at low temperature are shown in Figure 4-7.

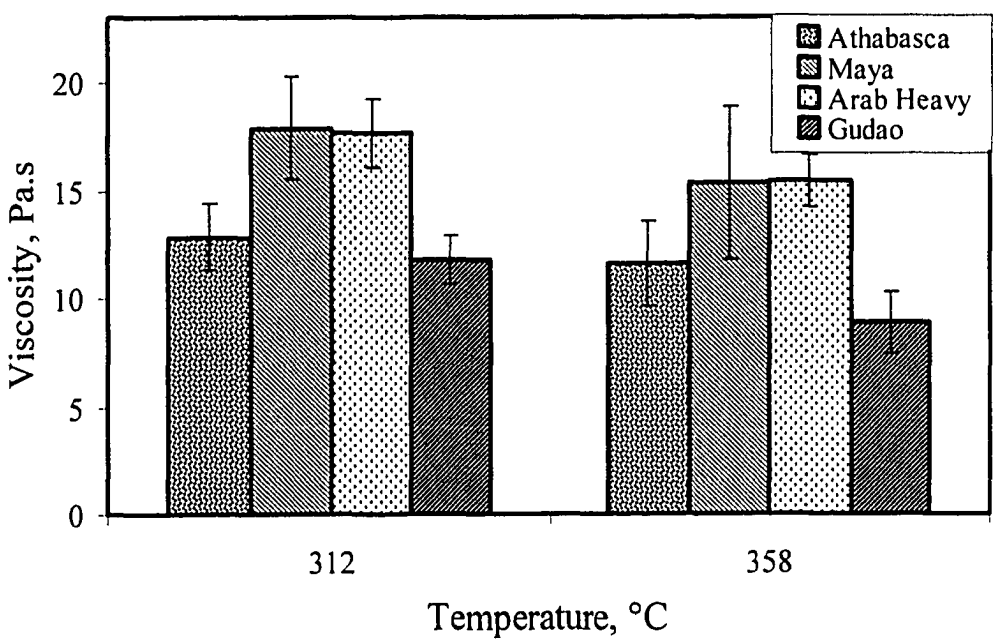

Figure 4-7. Viscosity of asphaltenes at low temperature (t_t = 15s)

The viscosity of all the asphaltenes decreased with the temperature as expected. As with the surface tensions, the viscosities for all the asphaltenes were in the same order of magnitude, with a difference between the lowest and highest viscosity of 6 Pa.s and 6.6 Pa.s at 312 and 358 °C, respectively. However, some statistical differences were found between the samples (to 95% of confidence). At 312 °C there are two pairs of similar results; the high viscosities of the asphaltenes from Maya VR and Arab Heavy VR and the lower viscosities of the asphaltenes from Athabasca VR and Gudao VR. At 358 °C the same trend was observed, but the viscosity of the asphaltene from Gudao VR was significantly lower. The low viscosity of the Gudao VR asphaltenes, relative to the other samples, can be explained based on the higher paraffinic and cycloparafinic carbon content (see Table 2-3). The differences in the results of viscosity for the other asphaltenes were not correlated with any chemical or structural characteristics.

Storm et al. (1991), working under somewhat different experimental conditions, found that blends of deasphalted oil and asphaltenes from different sources also had the same intrinsic viscosities at 93 °C. Storm et al. (1991) justified this observation by suggesting that the heteroatoms, which differ in concentration between different asphaltenes, are buried inside the asphaltene particles or agglomerates. The motion of these agglomerates in the liquid oil will control the viscosity, therefore, the heteroatoms would have only a small influence on the hydrodynamics of the fluid. The same argument can be used to interpret the relatively narrow range of viscosity observed in Figure 4-7. Alternately, the

observation that all the viscosities were within a factor of 1.5 could be attributed to the similarities in the origin of the asphaltenes. All these materials were soluble in the initial crude and insoluble in *n*-heptane. Consequently, compositional variables such as nitrogen content and aromaticity fell in a relatively narrow range (Tables 2-2 and 2-3).

4.2.2 VISCOSITY OF BLENDS OF AVR/AVR-ASPHALTENES

In a similar fashion to the viscosity measurement of asphaltenes, the same samples of Section 4.1.2 were used to measure the viscosity of the blends of AVR with AVR-asphaltenes. The results are shown in Figure 4-8.

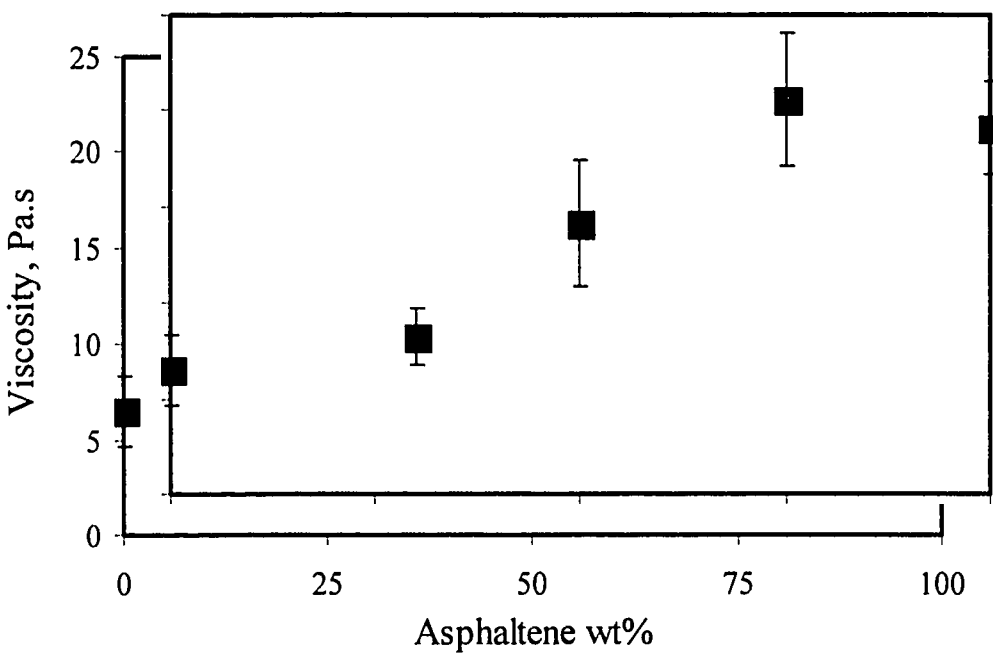

Figure 4-8. Viscosity of Athabasca VR/Athabasca VR asphaltenes blends versus weight percent of asphaltene at 503 °C (t_t = 15s). The x-axis indicates the initial composition of the blend (t = 0)

Figure 4-8 shows that the viscosity of the Athabasca VR generally increased with the asphaltene weight fraction. Specifically, the change was seen between circa 30 and 75 wt % of asphaltenes. Below 30 wt % and above 75 wt %, no statistical change was observed (95% of confidence interval). Despite the fact that the composition was known to have a relatively strong influence on the viscosity of bitumen (Mehrotra et al., 1989, Werner et al., 1998a, 1998b), the specific trend of the viscosity of the Athabasca VR with the asphaltene content under these conditions was unknown. As shown previously in this chapter, the viscosity of the asphaltenes was higher than the viscosity of the AVR. In consequence, an increase of the viscosity was expected as the asphaltene content increased. Also, results available under different conditions from Dealy (1979), Werner et al. (1998b), and Rayes et al. (2002), showed a strong increase of viscosity with the asphaltenes content for oil and bitumen mixtures between 25 and 100 °C. Altgelt and Harle (1975) also observed an increase of the viscosity of asphalts with the addition of asphaltenes.

An interesting and unexpected feature of these results (Figure 4-8) is that the viscosity of the AVR blends was not affected by the asphaltene content at the extreme concentrations. Above ca. 75 wt % asphaltenes, the viscosity was dominated by the asphaltenes, so the blend behaved as "pure" asphaltenes. Hence, any further increase of the asphaltenes content did not affect the viscosity. This explanation does not agree with the well-known strong effect on viscosity that diluents have on viscous material at lower temperatures, e.g. the addition of

naphtha to reduce the viscosity of bitumen. When we consider the temperature at which the measurements were done, then the compositional behavior makes more sense. At 503 °C all the possible traces of diluents in the sample are gone and the light components that could being produced by cracking reactions pass into the vapor phase relatively fast, at least in the liquid bridge that is the zone where the fluids properties are measured. Consequently, all of the components would be relatively high molecular weight with high viscosity.

On the other hand, at concentrations of asphaltenes below ca. 30 wt %, the relatively constant viscosity is also difficult to explain. One factor that could affect the results was the way the film thickness of the asphaltenes-free sample was calculated. As mentioned in Section 3.4.4, the film thickness of the coat on the rod at t_v is required to calculate the viscosity. A kinetic model based in the analogy in the chemistry between the AVR and its asphaltenes was used to calculate the film thickness. This kinetic model works within the experimental error for the samples initially containing asphaltenes, but in the case of the asphaltenes-free (maltenes) sample it might not be accurate. For this reason, a sensitivity analysis of the influence of the kinetic model on the viscosity results was performed. The difference between the viscosity results using different kinetic approaches was less than 1 %. A similar analysis with the same results was done to study the influence of the density on the calculated initial film thickness. The density used for the maltenes sample was calculated under the assumption of additives volumes, but a

range of densities from 1000 to 1100 kg/m^3 had no significant effect on the calculated viscosity.

To estimate the effect of the asphaltenes on the viscosity of the reacting system, the viscosities of the AVR and AVR-asphaltenes at 503 °C before reacting were estimated by extrapolation. The AVR data from the RMS shown in Figure 4-5 was fitted using a double-logarithmic equation giving a viscosity of ca. 0.006 Pa.s at 503 °C. For the AVR-asphaltenes, the data at 312, 358, and 400 °C (shown in the same figure) was fitted in the same way giving a viscosity of ca. 7 Pa.s at 503 °C. These estimates clearly show than even before the cracking reactions start, the viscosity of the asphaltene material was greater than the residue by approximately 3 orders of magnitude. This notable difference in the magnitude of the viscosities at t = 0 also indicated that something more than the volatilization of the lighter components was responsible for the change of the viscosity at short times. As the temperature increases, even after reaching the onset of cracking reactions, other reactions such as polymerization in the liquid phase must occur to account for the increase in viscosity. The initial asphaltene-free character of the sample (first data point of Figure 4-8) does not imply the absence of asphaltenic material at the time of the measurements (t_v) due to such polymerization reactions. Unfortunately, the characterization of the composition of the samples at the time of measurements, i.e. t_v, and t_s, as well as the transient rheological behavior of the samples with time, were beyond the scope of the present work.

4.2.3 Modeling the Viscosity of the AVR as a Function of Composition

Because of the experimental results presented in Section 4.2.2, and other evidence of the dependence of the viscosity on the composition (Werner et al., 1998b); the change of viscosity with the asphaltenes content at 503 °C was modeled using a standard mixing rule for viscosity (equation 2-1), using the mass fraction as the compositional variable. No interaction coefficients were included in equation 2-1 for simplicity. Other more complex expressions of the mixing rule have been used previously, such as Shu's equation (Schramm and Kwak, 1988), the Cragoe's equation used by Miadonye, et al. (2001), or a version of the Equation 2-1 used by Werner et al., (1998a) that includes ternary interaction coefficients (Equation 2-2). One more reason for using equation 2-1 was the uncertainty already present in the experimental results. A more sophisticated model would not necessarily give more accurate results from this limited set of data.

For the calculation of the viscosities, the two extreme compositions shown in Figure 4-8 were used. Thus, a mixture with 2 pseudocomponents was assumed, the reacted maltenes and the reacted asphaltenes. An expansion of Equation 2-1 gives Equation 4-2 where the sub-indexes stand for the two pseudocomponents.

$$\ln(\mu_m) = x_1 \ln(\mu_1) + x_2 \ln(\mu_2) \qquad (4\text{-}2)$$

Although it is known that a more complex expression could lead to better results, the simplicity of the Equation 4-2 should not be taken as too naïve since a linear combination of the contributions from asphaltenes and maltenes was obtained by Rahmani et al. (2002) when modeling the coke yield of the thermolysis of AVR/AVR-asphaltenes.

To illustrate the results from the model, the data points from Figure 4-8 are presented with the model in Figure 4-9. This figure shows that the measured viscosity can be predicted from the liquid-mixture model using initial asphaltene content as the compositional variable. The log-linear equation of the model is presented in Equation 4-3, where the X represents the initial weight percent of n-C_7-insoluble asphaltenes.

$$\ln(\mu_m) = 1.8881 + 0.0124X \qquad (4\text{-}3)$$

The model equation does not account for any kinetic effects on the viscosity. As pointed out clearly in Section 4.2.2, important changes due to reactions are likely to be taking place within the system well before reaching 503 °C. However, the aim of a model such as Equation 4-3 is to provide an estimate of the compositional effect on the viscosity, for example, for fluid coker units where approximate values of viscosity give insight about the dry-out time of the system (feed + hot coke particles) inside the reactor in the first 20 seconds of residence time.

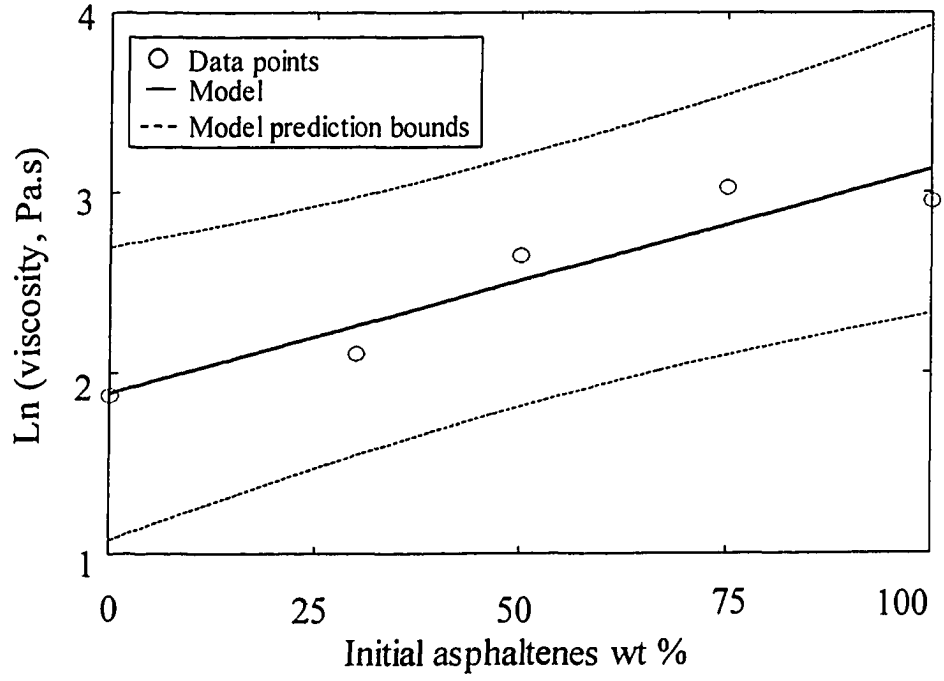

Figure 4-9. Model for the viscosity of AVR-asphaltenes as a function of composition at 503°C. Prediction bounds are at 95% of confidence level

4.3 CONTACT ANGLE

4.3.1 DYNAMIC CONTACT ANGLE OF ASPHALTENES ON SOLID SURFACES

The contact angle of the AVR-asphaltenes was measured on several surfaces using the method described in Section 3.4.3. The results are illustrated in Figure 4-10.

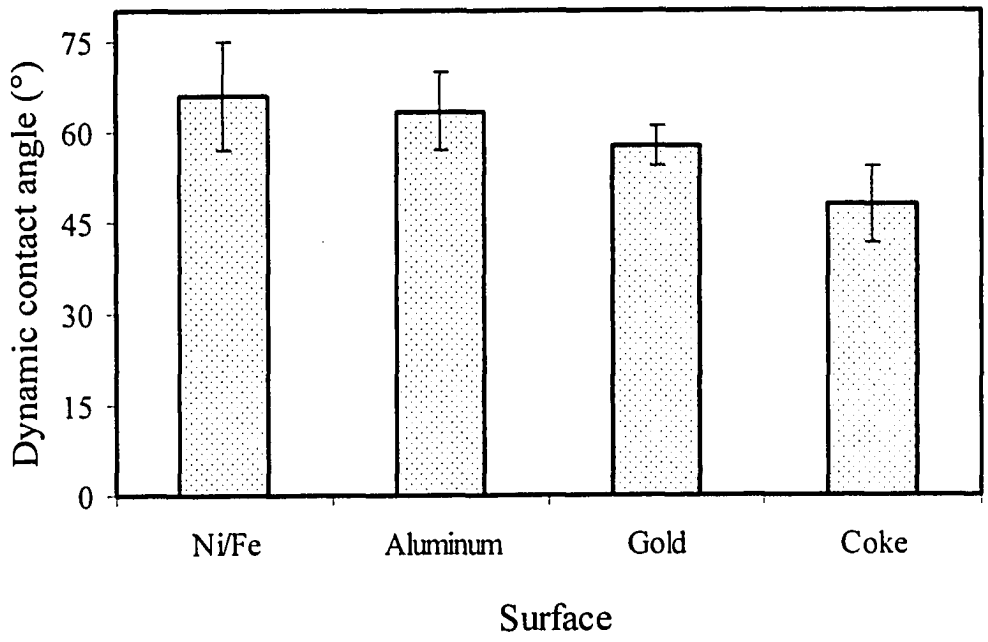

Figure 4-10. Dynamic contact angle of AVR-asphaltenes on different solid surfaces (temperature 250 – 300 °C)

The relation between contact angle and wettability and adhesion was reviewed in Section 2.4.3. The smaller the contact angle, the better the wettability of the solid by the liquid in contact with it under the experimental conditions. Hence, Figure 4-10 illustrates a measurement of the wettability of the AVR-asphaltenes on different surfaces at the experimental conditions. Clearly it can be observed that the wettability of the Ni/Fe alloy was the poorest and the wettability of the coke the best, with the aluminum and gold giving intermediate results. The average contact angle on Ni/Fe was 66.1°, on coke 47.9°, and on aluminum (63.5°) slightly larger than on gold (57.7°). The results show that the liquid asphaltenes will tend to adhere to all of these surfaces, given that contact angles are all < 90° under the experimental conditions. This result indicates that fouling by asphaltenic material may be affected by the surface properties, with coke or other organic deposits giving the highest affinity.

As with the surface tension and the viscosity, the results for contact angles of the AVR-asphaltenes were compared with result for other asphaltenes. Given the results from Figure 4-10, the surfaces with the poorest and the best wettability (Ni/Fe and coke) were selected to conduct the same measurements with the other 3 asphaltenes. Figure 4-11 shows the results on these two surfaces for all the asphaltenes. The data from Figure 4-11 show statistically significant differences (95% confidence interval) between the results on the two surfaces for each of the asphaltenes, implying in consequence a difference in wettability. All the asphaltenes showed a better wetting on the coke surface, which was consistent with

the chemical similarity between the coke and the asphaltenes. The range of results for the coke was circa 14°, and for the Ni/Fe it was circa 12°. Even though these are relatively small ranges of variation, the results from asphaltenes from Maya VR were statistically larger than the rest of the samples on both surfaces (95% confidence interval).

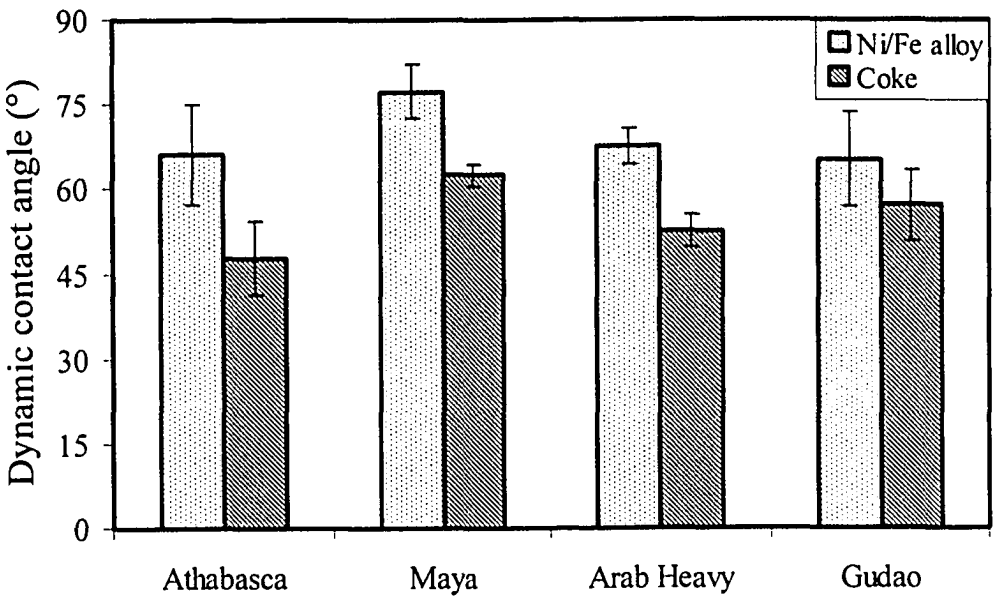

Figure 4-11. Dynamic contact angle of asphaltenes on coke and Ni/Fe alloy

Upon review of the results, it is important to comment on the dynamic character of the results shown in Figures 4-10 and 4-11. As discussed in Section 3.4.3, the contact angle was measured using Equation 3-2 right after observing the apparent complete melting of the asphaltenes, but some conditions must be fulfilled for the Young equation (Equation 2-3) to be valid. Equation 2-3 is valid only at the equilibrium condition, or when no forces other than γ_s, γ_{sl}, and γ_l are present, and there is no motion of the droplet during the measurement of the angle θ (Cao et al. 2002). The condition of equilibrium and no motion is fulfilled relatively easily for low viscosity liquids. But the results from in Section 4.2 show that asphaltenes are far from being low viscosity liquids, with viscosities in the order of 15 Pa.s at 312 °C. Hence, when a droplet is in motion during the measurement, the angle observed is the dynamic contact angle. Consequently the results from Figures 4-10 and 4-11 should be considered dynamic contact angles, due to the high viscosity and short time for measurements.

Another important consideration is the roughness of the surfaces. Formally, for the true contact angle to be measured a completely flat surface is necessary, otherwise the angle measured is an apparent contact angle (Wenzel, 1936). The surfaces of the gold, aluminum and Ni/Fe were carefully cleaning and the coke-coated rods were kept away from any dusty environment, but no other polishing procedure was performed; nor was the surface roughness measured. While surface roughness could have some impact on the reported results, the high viscosity and short time (5 – 10 seconds) for equilibration have much more significant effect on

the contact angle measurements. Hence, all the surfaces were assumed to be flat and smooth.

4.3.2 Equilibrium Contact Angle of Asphaltenes on Solid Surfaces

Given all the difficulties to relate dynamic contact angles with their respective equilibrium values (Bracke et al., 1989), equilibrium contact angles were measured directly for the 4 asphaltenes on Ni/Fe and on coke surfaces. The results are presented in Figure 4-12. The asphaltenes melts were allowed to spread on the solid surfaces for at least 120 seconds. The measurements of contact angle were taken once the equilibrium was reached, between 120 – 180 seconds. The equilibrium condition was verified when no further change in the dimensions of the drop were observed. The time to reach the equilibrium was considerably longer than the time used to measure the dynamic contact angle, reaffirming the strong effect of the surface tension and viscosity on the contact angle measurements discussed in Sections 2.3.3 and 4.3.1.

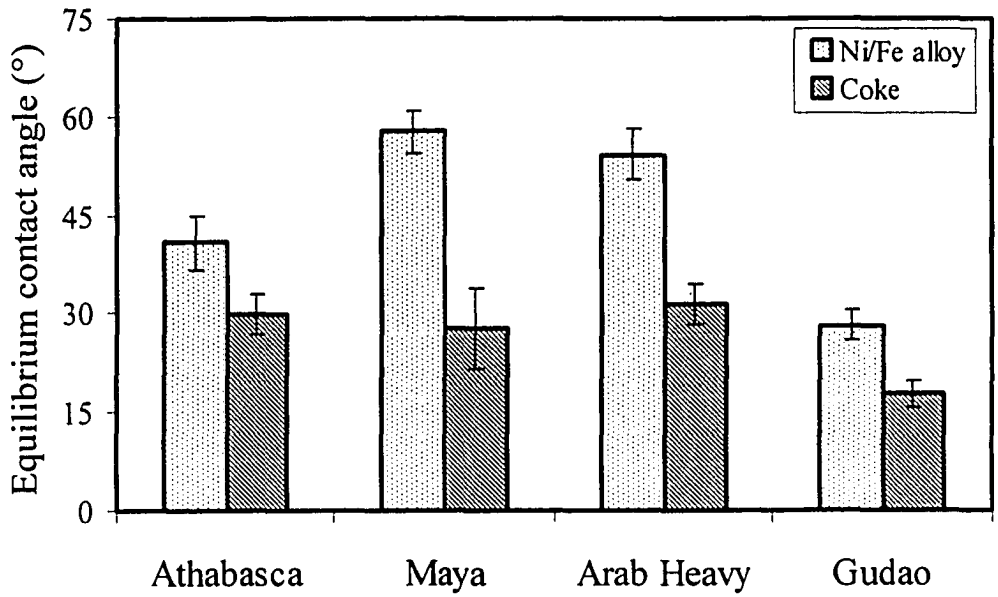

Figure 4-12. Equilibrium contact angle of asphaltenes on coke and Ni/Fe alloy

The results from Figure 4-12 show a statistical difference between the two surfaces for each of the asphaltenes. The wettability of the coke was better than the Ni/Fe. Furthermore, the difference between the results for these two surfaces was slightly larger than in the dynamic measurements. As expected, the measured equilibrium contact angles were smaller overall than the dynamic values. The maximum angle was 57.7° (Maya VR-asphaltenes on Ni/Fe) in contrast with the dynamic results in which only two angles were below 57°. The results for the equilibrium contact angle showed that the wettability of the Ni/Fe and coke was improved with increased time for measurement. As the asphaltenes were allowed to spread on the surface, the adhesion improved. Some experimental angles were practically impossible to measure, i.e. almost zero, during some of the equilibrium

contact angle measurements on coke, but these observations were outliers and were not repeatable.

Even though the contact angle did not change from 180 to 0 ° during the experiments, as assumed in Section 2.3.3, a qualitative relaxation time was calculated using the data of surface tension and viscosity at 312 °C, and an average radius of the droplets of 7.10^{-4} m, determined from the geometry of the melted drops. The predicted relaxation times were in the order of 10 – 20 seconds, and the results are presented in Table 4-1. As mentioned before in this section, the liquid drops were allowed to spread for at least 120 seconds, so the relaxation times shown in Table 4-1 confirmed that the equilibrium condition for the contact angle was reached, given the surface tension and viscosity of the asphaltenes. According to Table 4-1, the asphaltenes from Gudao VR and Athabasca VR reached the equilibrium stage relatively faster than the other two asphaltenes, based on the fluid properties measured by the liquid bridge technique.

Table 4-1. Comparison relaxation times of the dynamic contact angle of asphaltenes on solid surfaces

Sample	Surface Tension at 312 °C, mN m^{-1}	Viscosity at 312 °C, Pa.s	Relaxation time, s
Athabasca VR	20.70	12.83	11
Maya VR	19.72	17.90	16
Arab Heavy VR	17.58	17.67	18
Gudao VR	20.48	11.80	10

The relation between contact angle and adhesion is well established, and its role in fouling by asphaltenes has been suggested by Watkinson and Wilson (1997) and Watkinson and Asomaning (2000). Adhesion is a necessary step in the deposition of asphaltenes on solid surfaces as mentioned by Rao (2001). Unfortunately, as explained in Section 2.4.3, no results of contact angle of asphaltenes under these conditions could be found. Hence, no further comparison can be made to validate the results presented here.

4.4 Effect of AVR-Bitumen Solids on the Fluid Properties

Due to the high load of insoluble solids present in the Athabasca bitumens from surface mining, and thus in the Athabasca VR, the surface tension and viscosity of the Athabasca VR with and without the bitumen solids were measured. The data for the fluids properties of the Athabasca vacuum residue with the solids, or whole AVR were taken from Aminu (2003). The same temperature range of Sections 4.1 and 4.2 was used for these measurements, from 312 to 530 °C.

The results for the surface tension are illustrated in Figure 4-13. The trend of the surface tension with temperature is the same for both cases. The surface tension decreased by 12 – 15 mN/m from 312 to 530 °C. The decrease of the surface tension with temperature was discussed in Section 4.1. The results with and without solids were not only in the same order of magnitude but also were practically the same within the experimental error. Brian and Chen (1987) and

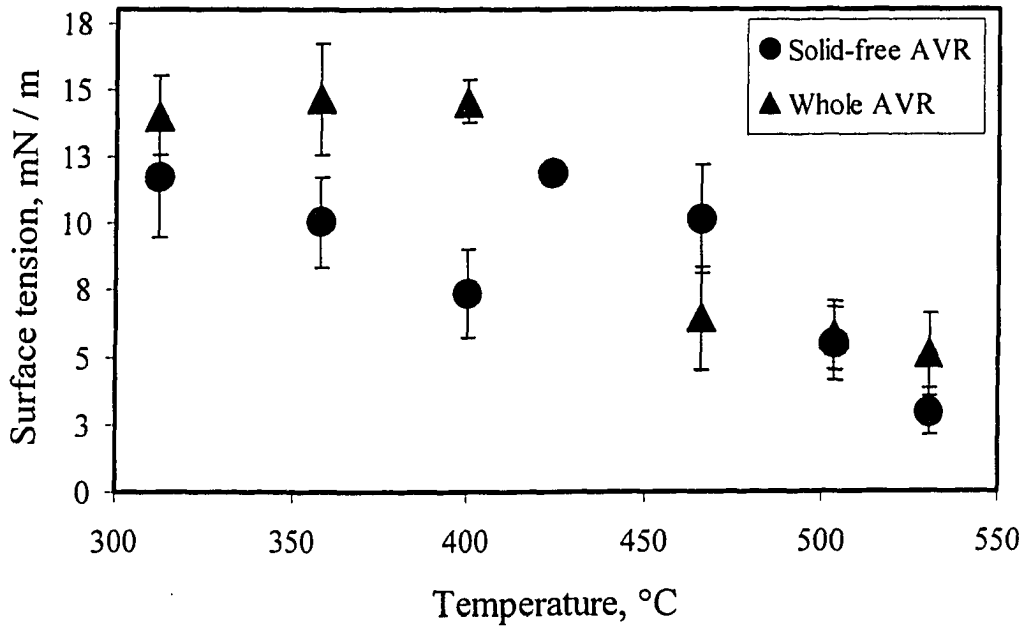

Figure 4-13. Surface tension of solid-free AVR (■) and of whole AVR (Aminu, 2003; data for selected times ▲) at t_t = 15s

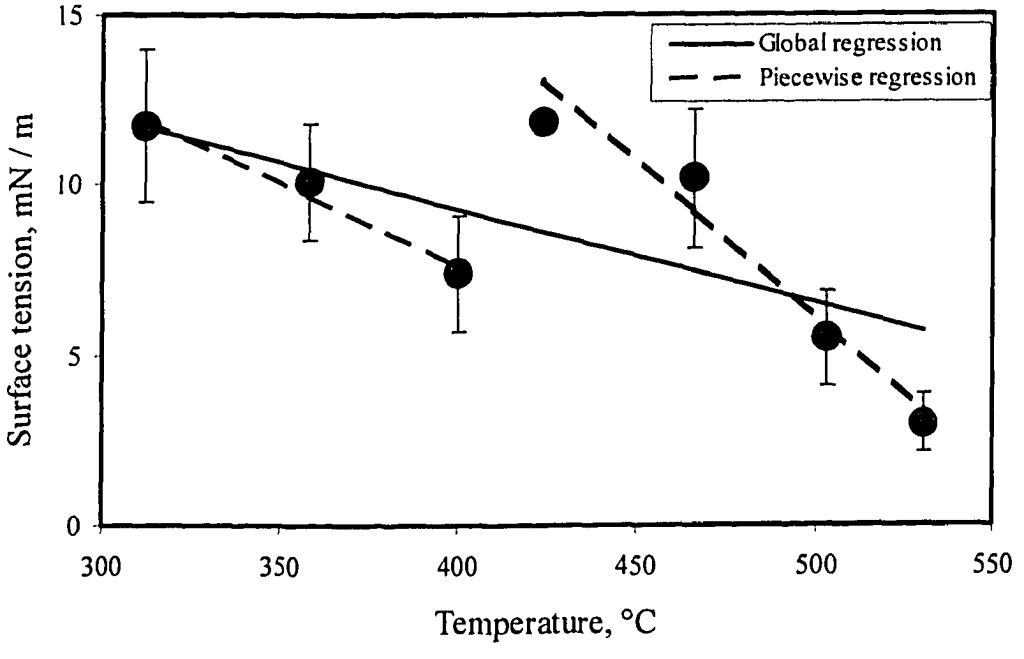

Figure 4-14. Surface tension of solid-free AVR versus temperature (t_t = 15s)

Vargha-Butler et al. (1988) studied the role of the solids in the surface tension of bitumen, but no evidence of change in the surface tension due to the presence of solids were found. Furthermore, Brian and Chen (1987) obtained the same results of surface tension when 0 up to 45 wt % of solid particles with sizes from 0.5 to 106 μm were added to a liquid paraffin. They claimed that since the surface tension is a molecular effect, only when the solid particles are of the size of the liquid molecules would the particles affect the surface tension. Brian and Chen (1987) and Vargha-Butler et al. (1988) used much lower temperatures than 312 – 530 °C, but the conclusion would extend to higher temperatures. In this work the equivalent surface tension between the two VR samples is justified based on two key factors. First, the solids were not molecularly distributed, given low colligative effects. Second, the interactions between solids were weak, which means a large number of liquid molecules were in between the solids, diminishing their effect on the surface tension.

The data of surface tension as function of temperature (Figure 4-13) were measured by the same technique as Aminu et al. (2004), but due to some improvements explained in Section 3.5.2 the detailed trend for the changes in surface tension with temperature was clearer for the solid-free AVR. The data of Figure 4-13 show that the surface tension with and without solids for AVR were generally consistent, decreasing from 13 mN/m at 312 °C to 4 mN/m at 530 °C. Isolating the results for the solid-free AVR, another very interesting feature can be seen, as shown in Figure 4-14.

Figure 4-14 shows that the decrease with temperature of the surface tension of the solid-free AVR was not uniform, due to a disruption in the linear trend somewhere between 400 and 424 °C. This was the range of temperatures where thermal reactions became significant for cracking of the AVR (Gray et al., 2004b). The surface tension decreased from 11.7 to 7.4 mN/m between 312 and 400 °C, and then increased to 11.9 mN/m at 424 °C, then decreased again to ca. 3 mN/m at 530 °C. A global linear regression and a piecewise regression are shown in Figure 4-13. The slopes of the two piecewise regressions were statistically different (at a 95% of confidence), and they are shown in Table 4-2. The significant difference between the slopes confirmed that the surface tension of the solid-free AVR was not a monotonic function of the temperature.

From the data of Table 4-2, 3 different slopes defined the decrease of surface tension of the AVR with temperature, each one for a different temperature regime. Initially, according to Li et al. (2003), $d\gamma/dT$ was –0.0376 mN m^{-1} $°C^{-1}$ in the range 150 – 280 °C, then it changed to – 0.0447 mN m^{-1} $°C^{-1}$ in the range 312 – 400 °C, and finally increased again to – 0.092 mN m^{-1} $°C^{-1}$ between 424 and 530 °C. No report of this kind of sudden jump or anomaly in the surface tension of the asphaltenes or vacuum residues as the temperature increases could be found. However, Chan et al. (2003) reported a very similar disruption of the surface tension for high-density polyethylene melts in the range of 200 – 230 °C. They suggested that the discontinuities in surface tension were due to structural rearrangements, analogous to liquid crystals.

Table 4-2. Comparison of linear regression slopes from surface tension versus temperature data.

Sample	Slope, mN m^{-1} $°C^{-1}$	Temperature range, °C	Source of data
Athabasca bitumen[1]	-0.095	64 – 112	Isaac and Smolek (1983)
Athabasca bitumen[2]	-0.076	40 – 90	Potoczny et al. (1984)
Utah bitumen	-0.082	40 – 83	Drelich et al. (1994)
AVR[3]	-0.0376	150 – 280	Li et al. (2003)
AVR	-0.0447	312 – 530	Aminu (2003)
Solid-free AVR	-0.049 -0.092	312 – 400 424 – 530	this work
AVR-asphaltenes	-0.072	312 – 530	this work

[1] solvent extracted, [2] extracted by centrifuging, [3] dynamic values (at 46 seconds).

In regard to the slope of the curve of the surface tension of the AVR-asphaltenes, as mentioned in Section 4.1.1 the data used were dynamic values. However, as Yarranton et al. (2000) pointed out, equilibrium surface tensions are not required to obtain the slope $d\gamma/dT$. The data in Table 4-2 show that the surface tension of the AVR-asphaltenes changes faster with the temperature than the whole AVR and solid-free AVR samples at 312 – 400 °C. Actually, the slope from the regression for the AVR-asphaltenes is very close to slope for the bitumens and the solid-free AVR at 424 – 530 °C. Since the average sizes of the molecules that make the AVR and AVR-asphaltenes are larger than those from the whole bitumen (lighter components), these results disagree with the expectation that $-d\gamma/dT$ should decrease as the molecular size increases (Wu, 1982; Potocnzy et al., 1984).

Like the surface tension, the viscosity was not affected by bitumen solids as illustrated in Figure 4-15. The viscosity followed the same trend with and without solids and that the results were the same within experimental error. In all the studies reviewed for comparison, either the viscosity was measured for other bitumens (no significant solids content) or no effort was made to investigate the role of solids. The results of Figure 4-15 were as expected, because the volume fraction of solids was small given a content of 1.8 wt %. The volume fraction of solids would have to be larger to change the rheological properties of the liquid. These results are important since some debate is always associated with the bitumen solids present in the Athabasca bitumen and vacuum residue, especially related with coke yields in cracking reactions.

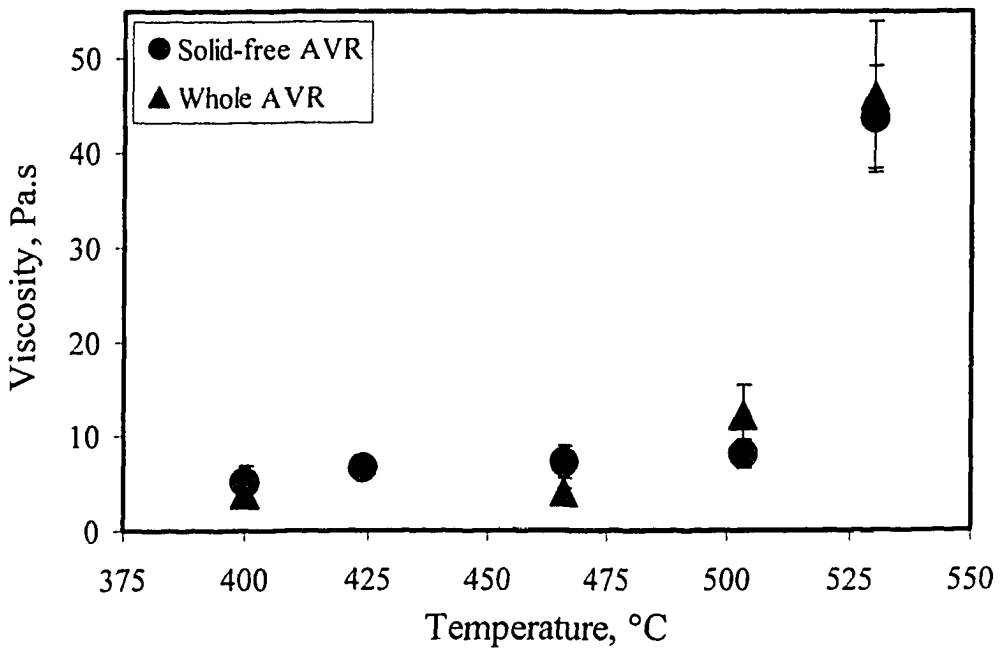

Figure 4-15. Viscosity of solid-free AVR (■) and of whole AVR (Aminu, 2003; data for selected times▲) at t_t = 15s

4.5 PROCESS IMPLICATIONS

The surface tension and viscosity are two very important properties in most of the equations for flow of fluids. The viscosity is one of the variables Reynolds number and the other dimensionless groups governing fluid behavior. In refining processes, the fluid viscosity determines the head losses and thus the pressure within units (Werner et al., 1998b). The variation of these properties with composition could have application in several fields related with the operation of refining and upgrading processes. The contact angle is related to fouling phenomena, a major concern of the petroleum industry. The role of the bitumen solids have been frequently debated, especially their implications in upgrading.

In the case of fluid-bed coking processes, the initial agglomeration of the coke particles inside the reactors likely depends on the initial fluid properties of the bitumen under the process conditions. Once the liquid is in the fluid bed, the formation and stability of agglomerates is a direct function of surface tension and viscosity as the reactions proceed, among other variables (Gray, 2002).

The findings of this work reported, for the first time, surface tension and viscosity of asphaltenes above 300 °C. More importantly, the liquid bridge technique was proven to be useful to measure the effect of composition on the fluid properties of heavy oils and bitumens liquids.

The variation of the surface tension and viscosity with composition, studied in this work through the asphaltene content, is also very important. Distillation columns and coking units are not isolated units within upgrading facilities. Prior

treatments, such as distillation and blending of recycle materials will affect the feed composition in residue conversion process. Any change in the feed composition may influence its properties, and in consequence product composition and yield. The effect of the composition is often neglected from data related with dynamic viscosity for petroleum systems (Werner et al., 1998a). In other words, despite the importance of feed composition, few studies have considered the importance of its impact on the fluid properties (Rahmani, 2003a). Having a model to at least estimate the behavior of the fluid properties as a function of composition and reaction conditions may be valuable in the design of feed systems to improve yields and minimize fouling. In particular, the model presented in Figure 4-9 is, as far as the author knows, the first of its kind. This model allows the prediction of the viscosity of a reacting mixture under specific conditions based on the initial asphaltene content. These results suggest that the fluid properties of the reacting bitumen in cokers will be relatively insensitive to changes in feed composition. In the thin film regime studied in these experiments, both the dry-out time and the fluid properties were dominated by the heaviest fractions of the oil. Changes in asphaltene content, due to upstream separation by distillation or solving deasphalting, would have little impact on fluid properties or kinetics, as a first approximation.

For process engineering and design calculations, a maximum value for the surface tension and viscosity of vacuum residue under certain conditions can be set based on the results of this work. As mentioned earlier in this chapter, Figure 4-6

clearly shows that the viscosity of the asphaltenes is higher than the vacuum residue for all the temperatures. The same is also observed for the surface tension, comparing Figures 4-1 and 4-13.

The knowledge gained from the study of the contact angle of asphaltenes may lead to a better understanding of the fouling mechanisms in different equipment. These mechanisms are known to be related to deposition, wetting, and adhesion phenomena (Watkinson and Wilson, 1997, Watkinson and Asomaning 2000), even though Wiehe et al. (2001) claimed that the insolubility of the asphaltenes is not necessary for the fouling of heated metals to occur. Additionally, because of the comparisons among several different asphaltenes, this work may allow successful mitigation of fouling for a specific process and feed to be generalized to other applications with different feeds. The results from this work demonstrated that the asphaltene melts wet better a coke than a metallic alloy surface. Consequently, the fouling of equipment due to asphaltenic material would be favoured by previous deposits of carbonaceous material on the walls of pipes and vessels. Other materials and conditions could be used to extend these results. For example, the contact angle for vacuum residue/asphaltenes blends could be measured on different surfaces to get an estimate of the wettability at conditions closer to the process conditions. The ultimate challenge would be to measure liquid-liquid solid contact angles under representative conditions.

All the work done in this study with asphaltenes is consistent with the comment made by Zhang et al. (2004). They explained that to successfully deal

with the fouling phenomena and to facilitate upgrading processes, it is necessary not only to know about the asphaltene chemical structure and composition but also its properties to provide insight into the behavior of asphaltenes under different conditions.

The knowledge obtained from the findings of this work about the role of the bitumen solids in the surface tension and viscosity of the Athabasca VR brings closure to one of the aspects of a particular issue with the Athabasca bitumen and vacuum residue. We can now generalize results on physical properties from Athabasca bitumen and its vacuum residue to other systems without paying special attention to the bitumen solids content.

5. CONCLUSIONS AND RECOMMENDATIONS

5.1 CONCLUSIONS

Based on the results obtained along this work regarding the fluid properties of asphaltenes between 310 and 530 °C, the following conclusions can be drawn:

1. The liquid bridge technique was proven to be useful to measure the surface tension and viscosity of asphaltenes and blends of vacuum residue and asphaltenes. Also, based on the used of the Curie-point alloy and an induction furnace, a new technique to measure the contact angle between asphaltene melts and solid surfaces was developed.

2. Between 312 and 530 °C, the surface tension of the AVR asphaltenes uniformly decreased at ca. 0.072 mN/(m °C), from 20.7 to 4.8 mN/m. Between 312 and 358 °C, asphaltenes from Athabasca VR showed similar results under the experimental conditions in comparison with asphaltenes from Arab Heavy VR, Maya VR, and Gudao VR. The surface tensions of all the asphaltenes were between 21 and 15 mN/m at 312 – 358 °C. At 503 °C, the surface tension of Athabasca VR was insensitive, within the experimental error, to the asphaltene content, over a range 0 to 100 wt % asphaltene.

3. Between 312 and 530 °C, the viscosity of the AVR asphaltenes presented two well-defined regimes. At lower temperatures, between 312 – 400 °C, the viscosity decreased at ca. 0.039 Pa.s/°C, from 12.8 to 9.3 Pa.s. At higher temperatures, between 424 – 530 °C, the viscosity measured at the experimental conditions increased from ca. 16 to 67 Pa.s. Within the lower temperature regime, the viscosity of the asphaltenes from Athabasca VR showed similar results under the experimental conditions to asphaltenes from Arab Heavy VR, Maya VR, and Gudao VR. The viscosities of all the asphaltenes were between 9 and 18 Pa.s at 312 – 358 °C. At 503 °C, the viscosity of Athabasca VR was affected by the asphaltene content, from 0 to 100 wt % asphaltenes. The most evident changed was observed between circa 30 and 75 wt % of asphaltenes.

4. For all the temperatures, AVR asphaltenes had a surface tension and viscosity greater than the AVR. The difference in surface tension was ca. 8 mN/m at 312 – 400 °C and ca. 2 mN/m at 424 – 530 °C. The difference in viscosity was ca. 10 Pa.s between 424 – 503 °C and ca. 20 Pa.s at 530 °C.

5. A predictive simple additive model to estimate the viscosity of the reacting mixture of AVR and AVR-asphaltenes at 503 °C was developed. The model predicts the viscosity based on the initial asphaltene content.

6. The dynamic contact angle between AVR asphaltene melts and different solid surface was measured. The observed dynamic contact angles were 47.9° on coke, 57.7° on gold, 63.5° on aluminum, and 66.1° on Ni/Fe alloy. The results of dynamic contact angle of Athabasca VR asphaltenes on coke and Ni/Fe alloy were found to be typical for asphaltenes when compared with dynamic contact angles of asphaltenes from Arab Heavy VR, Maya VR, and Gudao VR. The range of results for the coke was circa 14°, and for the Ni/Fe it was circa 12°.

7. Athabasca VR asphaltenes showed typical results for equilibrium contact angle, when compared to asphaltenes from Arab Heavy VR, Maya VR, and Gudao VR. Angles between 17.7 and 57.7° were observed.

8. The bitumen solids present in the AVR did not affect the fluid properties of the vacuum residue. The observed results of surface tension and viscosity with and without the mineral fines solids did not differ within the experimental error.

9. Between 312 and 530 °C, the surface tension of the solid-free AVR presented a disruption of the monotonic decrease between 400 – 424 °C. This anomaly was likely due to structural rearrangements at the liquid-vapor interphase.

5.2 RECOMMENDATIONS

Based on the results obtained along this work and its process implications, the following recommendations are proposed for the extension of the scope if this field of study.

1. The measurement of the fluid properties of samples obtained from bitumen after thermal treatment would help to generalize the results of this work. This study might set bounds to the value of surface tension and viscosity of the reacting system.

2. By combining the characterization of the composition of the samples during cracking with the study of the rheological behavior of the samples with time, the predictive model for the viscosity presented in this work (Equation 4-3) can be improved.

3. To obtain results more useful to fouling mitigation in industrial processes, contact angle between other solid surfaces and residue materials can be measured with the aim of generalizing the results presented here.

4. The influence of the traces of resins present in the separated asphaltenes on the melting behavior and fluid properties could be assessed by measuring the contact angle, surface tension and viscosity of asphaltenes prepared by more extensive washing procedures.

REFERENCES

Akhlaq, M.S., Götze, P., Kessel, D., and Dornow, W., "Adsorption of Crude Oil on Glass Plates: Measurements of Contact Angle and the Factors Influencing Glass Surface Properties". *Colloids and Surfaces,* **1997**, 126, 25-32

Al-Maamari, R.S.H., and Buckley, J.S., "Asphaltene Precipitation and Alteration of Wetting: the Potential for Wettability Changes During Oil Production", *SPE Reservoir Evaluation and Engineering*, **2003**, 6 (4), 210-214

Alboudwarej, H., Svrcek, W.Y., and Yarranton, H.W., "Sensitivity of Asphaltenes Properties to Separation Techniques", *Energy and Fuels*, **2002**, 16, 462-469

Altgelt, K.H., and Harle, O.L., "The Effect of Asphaltenes on Asphalt Viscosity", *Industrial & Engineering Chemistry Product Research and Development*, **1975**, 14 (4), 240-246

Aminu, M.O.,"Fluid Properties At Coking Process Conditions", MSc. Thesis, Chemical and Materials Engineering Department. University of Alberta. **2003**

Aminu, M.O., Elliott, J.A.W., McCaffrey, W.C., and Gray, M.R., "Fluid Properties At Coking Process Conditions", *Industrial & Engineering Chemistry Research*, **2004**, 43, 2929-2935

Basu, S., Nandakumar, K., Lawrence, S., and Masliyah, J., "Effect of Calcium Ion and Montmorillonite Clay on Bitumen Displacement by Water on glass Surface", *Fuel*, **2004**, 83, 17-22

Brian, B.W., and Chen, J.C., "Surface Tension of Solid-Liquid Slurries", *AIChE Journal*, **1987**, 33 (2), 316-318

Bryan, J., Mirotchnik, K., and Kantzas, A., "Viscosity Determination of Heavy Oil and Bitumen Using NMR Relaxometry", *Journal of Canadian Petroleum Technology*, **2003**, 42 (7), 29-34

Buckley, J.S., "Effective Wettability of Mineral Exposed to Crude Oil", *Current Opinion in Colloid & Interface Science*, **2001**, 6, 191-196

Budziak, C.J., Vargha-Butler, E.I., Hancock, R.G.V., and Neumann, A.W., "Study of Fines in Bitumen Extracted Oil Sands by Heat Centrifugation", *Fuel*, **1988**, 67, 1633-1638

Bussher, H.J., Van Plet, A.W.J., De Boer, P., De Jong, H.P., and Arends, J., "The Effect of Surface Roughening of Polymers on Measured Contact Angles of Liquids", *Colloids and Surfaces*. **1984**, 9, 319-331

Cao, J., Buckley, A.N., and Tomsett, A., "Re-examining the Pitch/Coke Wetting and Penetration Test", *Journal of the Mineral Metals & Materials Society*, **2002**, 54 (2), 30-33

Chan, C.C.V., Elliott, J.A.W., and Williams, M.C., "Interfacial Tension Measurements and Evidence of Order in High Density Polyethylen Melts", *Journal of Applied Polymer Science*, **2003**, 90, 4061-4067

Couderc, P., Hyvernay, P., and Lemarchand, J. L. "Correlations between Ability of Pitch to Penetrate Coke and the Physical Characteristics of Prebaked Anodes for the Aluminum Industry", *Fuel*, **1986**, 65, 281-287

Da Silva Ramos, C.A., Haraguchi, L., Notrispe, F.R, Loh, W., and Mohamed, R.S., "Interfacial and Colloidal Behavior of Asphaltenes Obtained from Brazilian Crude Oils", *Journal of Petroleum Science and Technology*, **2001**, 32, 201-216

Dealy, J.M., "Rheological Properties of Oil Sands Bitumens", *Canadian Journal of Chemical Engineering*, **1979**, 57, 677-683

Debacher, N.A., and Ottewill, R.H., "Kinetics of Contact Agnle Formation at the Gas-Liquid-Solid Interphase", *Colloids and Surfaces*, **1991**, 52, 149-161

Drelich, J., Bukka, K., Miller J.D., and Hanson, F.V., "Surface Tension of Toluene-Extracted Bitumen from Utah Oil Sands As Determined by Wilhelmy Plate and Contact Angle Techniques", *Energy and Fuels*, **1994**, 8, 700-704

Gent, A.N., and Hamed, G.R., "Adhesion" on Encyclopedia of Polymer Science and Technology, **2002**, Jhon Wiley & Sons, Inc

Gray, M.R., "Fundamentals of Bitumen Coking Processes Analogous to Granulation: A Critical Review", *Canadian Journal of Chemical Engineering*, **2002**, 80, 393-401

Gray, M.R., "Consistency of Asphaltene Chemical Structures with Pyrolisis and Coking Behavior", *Energy and Fuels*, **2003**, 17, 1566-1569

Gray, M.R., Assenheimer, G., Boddez, L., and McCaffrey, W.C., "Melting and Fluid Behavior of Asphaltene Films at 200-500 °C", *Energy and Fuels*, **2004a**, 18, 1419-1423

Gray, M.R., Le, T., McCaffrey, W.C., Berruti, F., Soundararajan, S., Chan, E., Huq, I. and Thorne, C., "Coupling of Mass Transfer and Reaction in Coking of Thin Films of an Athabasca Vacuum Residue", *Industrial and Engineering Chemistry Research*, **2001**, 40, 3317-3324

Gray, M.R., McCaffrey, W.C., Huq, I., and Le, T., "Kinetics of Cracking and Devolatilization During Coking of Athabasca Residues", *Industrial and Engineering Chemistry Research*, **2004b**, 43, 5438-5445

Gray, M.R., Zhang, Z., McCaffrey, W.C., Huq, I., Boddez, L., Xu, Z. and Elliott, J.A.W, "Measurement of Adhesive Forces During Coking of Athabasca Vacuum Residue", *Industrial and Engineering Chemistry Research*, **2003**, 42, 3549-3554

Gray, M.R., Zhao, Y., McKnight, C.M., Komar, D.A., and Carruthers, J.D., "Coking of Hydroprocessing Catalyst by Residue Fractions of Bitumen", *Energy and Fuels*, **1999**, 13, 1037-1045

Gloton, M.P., Turmine, M., Mayaffre, A., Letellier, P., and Toulhoat, H., "Study of Asphaltnes Adsorption on Mineral Surfaces by Contact Angle Measurements: Kinetics of Wettability Changes", *Physical Chemistry of Colloids and Interfaces in Oil Production*. Proceedings of the 6th IFP Exploration and Production Res. Conference held in Saint-Raphael, Sept. 4-6 1991. Published in **1992**

Isaac, E.E. and Smolek, K.F., "Interfacial Tension Behavior of Athabasca Bitumen/Aqueous Surfactant Systems", *Canadian Journal of Chemical Engineering*, **1983**, 61, 233-240

Johnson, S.E., Svrcek, W.Y., Mehrotra, A.K., "Viscosity Prediction of Athabasca Bitumen Using the Extended Principles of Corresponded States", *Industrial Engineering Chemistry and Research*, **1987**, 26, 2290-2298

Khan, M.B.A., Mehrotra, A.K., Svrcek, W.Y., "Viscosity Models for Gas-free Athabasca Bitumen", *Journal of Canadian Petroleum Technology*, **1984**, 23 (3), 47-53

Kotlyar, L.S., Sparks, B.D., and Woods, J.R., "Solids Associate with Asphaltene Fraction of Oil Sands Bitumen", *Energy and Fuels*, **1999**, 13, 346-350

Kopsch, H., "On the Thermal-Behavior of Petroleum Asphaltenes", *Thermochimica Acta*, **1994**, 235 (2), 271-275

Lahaye, J., and Ehrburger, P., "Pitch-Coke Interactions", *Fuel*, **1985**, 64, 1187-1191

Li, X., Elliott, J.A.W., McCaffrey, W.C., Yan, D., Li, D. and Famulak, D., "Dynamic Surface Tensions of Athabasca Bitumen Vacuum Residue", *Industrial and Engineering Chemistry Research*, **2003**, submitted

Mehrotra, A.K., "Modeling the Effects of Temperature, Pressure, and Composition on the Viscosity of Crude Oil Mixtures", *Industrial Engineering and Chemistry Research*, **1990**, 29, 1574-1578

Mehrotra, A.K., "A Model for the Viscosity of Bitumen/Bitumen Fractions-Diluent Blends", *Journal of Canadian Petroleum Technology*, **1992**, 31 (9), 28-32

Mehrotra, A.K., Eastick, R.R., and Svrcek, W.Y., "Viscosity of Cold Lake Bitumen and its Fractions", *Canadian Journal of Chemical Engineering*, **1989**, 67, 1004-1009

Mehrotra, A.K., Monnery, W.D., and Svrcek, W.Y., "A Review of Practical Calculation methods for the Viscosity of Liquid Hydrocarbons and their Mixtures", *Fluid Phase Equilibria*, **1996**, 117, 344-355

Miadonye, A., Doyle, N.L., Britten, A., Latour, N., and Puttagunta, V.R., "Modelling Viscosity and Mass Fraction of Bitumen-Diluent Mixtures", *Journal of Canadian Petroleum Technology*, **2001**, 40 (7), 52-57

Miadonye, A., Puttagunta, V.R., Srivastava, R., Huang, S.S., and Dafan, Y., "Generalized Oil Viscosity Model for the Effects of Temperature, Pressure and Gas Composition", *Journal of Canadian Petroleum Technology*, **1997**, 36 (1), 50-54

Mehrotra, A.K., Yee, C., and Svrcek, W.Y., "Prediction of Surface Tension of Athabasca Bitumen", *Canadian Journal of Chemical Engineering*, **1985**, 62, 340-343

Papirer, E., and Fritschy, G., "Modification of the Surface Properties of Bitumen and Asphaltenes Following Treatment with Sulfur at 140 °C", *Fuel*, **1981**, 60, 670-672

Papirer, E., Bourgeois, C., Siffert, B., abd Balar, H., "Chemical Nature and Water/Oil Emulsifying Properties of Asphaltenes", *Fuel*, **1992**, 61, 732-734

Perry, "Chemical Engineer's Handbook", electronic edition, **1999**, McGraw-Hill

Potoczny, Z.M., Vargha-Butler, E.I., Zubovits, T.K., Neumann, A.W., "Surface Tension of Bitumen. I. Temperature Dependence", *AOSTRA J. Res.* **1984**, 1, 107-115

Rahmani, S., McCaffrey, W.C., Dettman, H.D., and Gray, M.R., "Coking Kinetics and Asphaltenes as a Function of Chemical Structure", *Energy & Fuels*, **2003a**, 17, 1048-1056

Rahmani, S., McCaffrey, W., Elliott, J.A.W., and Gray, M.R., "Liquid-phase Behavior During the Cracking of Asphaltenes", *Industrial and Engineering Chemistry Research*, **2003b,** 42, 4101-4108

Rahmani, S., McCaffrey, W., and Gray, M.R., "Kinetics of Solvent Interactions with Asphaltenes During Coke formation", *Energy and Fuels*, **2002,** 16, 148-154

Rao, D., "Fluid-Fluid and Solid-Fluid Interfacial Interactions in Petroleum Resorvoirs", *Petroleum Science and Technology*, **2001**, 19, 157-188

Rayes, B.H., Pernyeszi, T., Lakatos, I., and Toth, J., "Comparative Study of Asphaltenes Adsorption on Formation Rocks under Static and Dynamic Conditions", *Progress in Mining and Oilfield Chemistry*, **2002**, 4, 257-273

Rogel, E., León, O., Torres, G., and Espidel, J., "Aggregation of Asphaltenes in Organic Solvents Using Surface Tension Measurements", *Fuel*, **2000**, 79, 1389-1394

Sheremata, J.M., Gray, M.R., Dettman, H.D., and McCaffrey, W.C., "Quantitative Molecular Representation and Sequential Optimization of Athabasca Asphaltenes", *Energy and Fuels*, **2004**, 18, 1377-1384

Sheu, E.Y., De Tar, M.M., Storm, D.A., and DeCanio, S.J., "Aggregation and Kinetics of Asphaltenes in Organic Solvents", *Fuel*, **1992**, 71, 299-302

Storm, D.A., Barresi, R.J., and DeCanio, S.J., "Colloidal Nature of Vacuum Residue", *Fuel*, **1991**, 70, 779-782

Streeter, "Handbook of Fluids Dynamics", McGraw-Hill, New York, **1961**

Tanabe, K., and Gray, M.R., "Role of Fine Solids in the Coking of Vacuum Residues", *Energy and Fuels*, **1997**, 11, 1040-1043

Varga-Butler, E.I., Zubovits, T.K., Budziak, C.J., Neuman, A.W., and Potoczny, Z.M., "Surface Tension of Bitumen from Contact Angle Measurements on Films of Bitumen", *Energy and Fuels*, **1988**, *2*, 653-656

Van Krevelen, D.W., "Property of Polymers", 3rd edition, **1997**, Elsevier, NY pp 227

Watkinson, A.P., and Asomaning, S., "Petroleum Stability and Heteroatom Species Effects in Fouling of Heat Exchangers by Asphaltenes", *Heat Transfer Engineering*, **2000**, *21*, 10-16

Watkinson, A.P., and Wilson, D.I., "Chemical Reaction Fouling: A Review", *Experimental Thermal and Fluid Science*, **1997**, *14*, 361-374

Wenzel, R.N., "Resistant of Solid Surfaces to Wetting by Water", *Industrial Engineering Chemistry*, **1936**, 28, 988-994

Werner, A., de Hemptinne, J.C., Behar, F., Behar, E., and Boned, C., "A new Viscosity Model for Petroleum Fluids with high Asphaltenes Content", *Fluid Phase Equilibria*, **1998a**, 147, 319-341

Werner, A., de Hemptinne, J.C., Behar, F., Behar, E., and Boned, C., "Viscosity and Phase Behavior of Petroleum Fluids with High Asphaltene Content", *Fluid Phase Equilibria*, **1998b**, 147, 343-356

Wiehe, I.A., Kennedy, R.J., and Dickakian, G., "Fouling of Nearly Incompatible Oils", *Energy and Fuels*, **2001**, 15, 1057-1058

Wu, S. Polymer Interface and Adhesion. Marcel Dekker, Inc. New York and Besel. **1982**

Yarranton, H.W., Alboudwarej, H., and Jakher, R., "Investigation of Asphaltenes Association with Vapor Pressure Osmometry and Interfacial Tension Measurements", *Industrial and Engineering Chemistry Research*, **2000**, 39, 2916-1924

Zhang, Y., Takanohashi, T., Sato, S., and Saito, I., "Observation of Glass Transition in Asphaltenes", *Energy and Fuels*, **2004**, 18, 283-284

Zuo, R., and Liu, L., "Role of Asphaltenes in Petroleum Cracking and Refining", on Asphaltenes and Asphalts, Part 1, edited by Yen, T.F., and Chiligarian, G.V., **1994**, Elsevier Science, New York.

APPENDIX A

EXPERIMENTAL DATA

A1 SURFACE TENSION AND VISCOSITY

A1.1 SURFACE TENSION AND VISCOSITY OF SOLID-FREE AVR

	Time, s	Surface Tension, m N / m	Time, s	Viscosity, Pa.s
T = 312 °C				
Series 1	16.5	11.9		
Series 2	16.7	15.2		
Series 3	16.8	12.1		
Series 4	16.8	9.4		
Series 5	18.3	10.1		
Average*	17.0 ± 0.7	11.7 ± 2.3		
T = 358 °C				
Series 1	14.1	8.9		
Series 2	17.3	12.2		
Series 3	15.4	11.1		
Series 4	16.5	10.2		
Series 5	16.9	7.8		
Average*	16.0 ± 1.3	10.1 ± 1.7		
T = 400 °C				
Series 1	14.5	6.8	14.6	4.4
Series 2	16.7	9.1	16.6	6.6
Series 3	16.6	5.8	16.7	3.7
Series 4	16.5	5.9	16.7	2.8
Series 5	16.7	9.2	16.9	6.9
Series 6			16.9	6.1
Average*	16.2 ± 1.0	7.4± 1.4	16.4 ± 0.9	5.1 ± 1.7

*Error expressed as standard deviation when more than three series were performed

A1.1 SURFACE TENSION AND VISCOSITY OF SOLID-FREE AVR (CONTINUED)

	Time, s	Surface Tension, m N / m	Time, s	Viscosity, Pa.s
T = 424 °C				
Series 1	11.9	12.5	17.2	6.5
Series 2	11.9	12.2	17.2	6.6
Average*	11.9	12.4 ± 0.2	17.2	6.6 ± 0.1
T = 466 °C				
Series 1	13.5	7.3	13.6	5.1
Series 2	16.9	9.8	17.0	5.1
Series 3	17.0	10.5	17.0	7.8
Series 4	17.0	13.1	17.2	8.9
Series 5	16.6	10.1	16.8	6.4
Series 6			17.0	7.0
Series 7			17.1	7.5
Series 8			16.7	10.6
Series 9			17.1	7.5
Series 10			16.6	6.0
Average*	16.2 ± 1.5	10.2 ± 2.1	16.6 ± 1.1	7.2 ± 1.7
T = 503 °C				
Series 1	16.4	7.4	16.5	5.9
Series 2	16.9	4.4	17.0	5.4
Series 3	17.0	5.7	17.2	9.1
Series 4	17.0	4.6	17.1	6.8
Series 5			17.2	8.3
Series 6			18.4	7.3
Series 7			17.7	6.5
Series 8			17.3	5.4
Average*	16.8 ± 0.3	5.5 ± 1.4	17.3 ± 0.6	6.9 ± 1.4

*Error expressed as standard deviation when more than three series were performed

A1.1 SURFACE TENSION AND VISCOSITY OF SOLID-FREE AVR (CONTINUED)

	Time, s	Surface Tension, m N / m	Time, s	Viscosity, Pa.s
T = 530 °C				
Series 1	13.4	2.4	16.8	37.1
Series 2	13.4	3.6	19.0	48.4
Series 3			26.2	48.1
Series 4			23.5	41.3
Average*	13.4	3.0 ± 0.9	21.4 ± 4.3	43.7 ± 5.5

*Error expressed as standard deviation when more than three series were performed

A1.2 SURFACE TENSION AND VISCOSITY OF AVR ASPHALTENES

	Time, s	Surface Tension, m N / m	Time, s	Viscosity, Pa.s
T = 312 °C				
Series 1	17.0	19.1	17.6	13.4
Series 2	17.0	21.8	17.4	11.8
Series 3	16.4	21.6	18.0	15.1
Series 4	16.7	20.3	17.4	13.9
Series 5			16.8	10.6
Series 6			17.6	11.7
Series 7			17.1	13.4
Average*	16.7 ± 0.3	20.7 ± 1.2	17.4 ± 0.4	12.8 ± 1.5

*Error expressed as standard deviation when more than three series were performed

A1.2 SURFACE TENSION AND VISCOSITY OF AVR ASPHALTENES (CONTINUED)

	Time, s	Surface Tension, m N / m	Time, s	Viscosity, Pa.s
T = 358 °C				
Series 1	17.1	18.4	18.1	12.3
Series 2	16.4	21.2	16.9	10.2
Series 3	16.8	17.6	17.8	13.0
Series 4	17.2	15.6	18.1	8.9
Series 5	17.3	21.5	18.2	14.6
Series 6			17.7	10.2
Series 7			18.8	12.2
Average*	17.0 ± 0.4	18.8 ± 2.5	17.9 ± 0.6	11.6 ± 2.0
T = 400 °C				
Series 1	15.7	16.3	15.7	9.6
Series 2	17.0	18.7	17.0	9.2
Series 3	17.0	15.5	17.1	11.2
Series 4	15.7	9.3	16.7	7.2
Average*	16.6 ± 0.8	14.9 ± 4.0	16.6 ± 0.7	9.3 ± 1.7
T = 424 °C				
Series 1	8.1	10.3	17.9	15.5
Series 2	8.1	14.2	17.4	19.9
Series 3	9.8	16.5	17.6	17.0
Series 4			17.9	11.6
Series 5			17.8	15.9
Series 6			17.9	15.5
Average*	8.7 ± 1.0	13.7 ± 3.1	17.7 ± 0.2	16.0 ± 3.0

*Error expressed as standard deviation when more than three series were performed

A1.2 Surface Tension and Viscosity of AVR asphaltenes (continued)

	Time, s	Surface Tension, m N / m	Time, s	Viscosity, Pa.s
T = 466 °C				
Series 1	17.5	12.9	17.7	13.1
Series 2	17.0	11.8	17.3	19.5
Series 3	17.2	15.4	17.8	21.5
Series 4	16.8	8.8	17.5	17.6
Series 5			17.3	14.4
Series 6			17.2	11.8
Average*	17.1 ± 0.3	12.2 ± 2.8	17.5 ± 0.2	16.3 ± 3.9
T = 503 °C				
Series 1	17.2	7.2	18.0	21.0
Series 2	22.2	9.2	17.6	21.9
Series 3	16.6	6.5	17.6	16.1
Series 4	17.0	6.6	17.5	19.0
Series 5			17.5	17.5
Average*	18.3 ± 2.7	7.4 ± 1.2	17.6 ± 0.2	19.1 ± 2.4
T = 530 °C				
Series 1	9.9	2.5	27.2	68.1
Series 2	12.7	6.7	28.1	69.9
Series 3	12.8	5.1	27.1	62.9
Series 4				
Series 5				
Series 6				
Average*	8.2 ± 1.2	4.8 ± 2.1	27.5± 0.5	67.0 ± 3.6

*Error expressed as standard deviation when more than three series were performed

A1.3 Surface Tension and Viscosity of Maya VR asphaltenes

	Time, s	Surface Tension, m N / m	Time, s	Viscosity, Pa.s
T = 312 °C				
Series 1	16.6	19.9	16.9	19.2
Series 2	16.8	21.6	17.5	20.3
Series 3	16.1	17.1	18.5	19.3
Series 4	16.8	20.3	16.5	15.6
Series 5			17.6	15.1
Average*	16.6 ± 0.4	19.8 ± 1.9	17.4 ± 0.8	17.9 ± 2.4
T = 358 °C				
Series 1	17.4	16.2	18.3	16.6
Series 2	17.5	20.3	18.1	20.8
Series 3	17.1	16.7	17.8	11.5
Series 4	16.9	19.8	17.6	14.1
Series 5	17.5	17.7	18.4	13.8
Average*	17.3 ± 0.3	18.2 ± 1.8	18.0 ± 0.3	15.3 ± 3.5

*Error expressed as standard deviation when more than three series were performed

A1.4 Surface Tension and Viscosity of Arab Heavy VR asphaltenes

	Time, s	Surface Tension, m N / m	Time, s	Viscosity, Pa.s
T = 312 °C				
Series 1	16.4	17.7	17.4	17.8
Series 2	16.7	19.7	17.5	16.0
Series 3	16.4	15.3	17.2	16.0
Series 4	16.4	18.6	16.8	19.6
Series 5	16.1	16.6	16.6	18.9
Average*	16.4 ± 0.2	17.6. ± 1.7	17.1 ± 0.4	17.7 ± 1.6
T = 358 °C				
Series 1	16.2	14.1	17.7	16.3
Series 2	17.0	13.4	17.9	15.8
Series 3	18.4	16.4	18.7	14.0
Series 4	17.6	16.0	18.3	14.9
Series 5	16.4	14.0	17.1	17.3
Average*	17.1 ± 1.0	14.8 ± 1.3	17.9 ± 0.6	15.7 ± 1.3

*Error expressed as standard deviation when more than three series were performed

A1.5 Surface Tension and Viscosity of Gudao VR asphaltenes

	Time, s	Surface Tension, m N / m	Time, s	Viscosity, Pa.s
T = 312 °C				
Series 1	17.1	18.2	17.3	11.2
Series 2	16.7	23.7	16.8	12.9
Series 3	16.9	19.6	17.1	11.2
Series 4			16.9	10.7
Series 5			17.2	13.1
Average*	16.9 ± 0.2	20.5. ± 2.9	17.1 ± 0.2	11.8 ± 1.1
T = 358 °C				
Series 1	8.5	17.0	16.8	8.3
Series 2	21.8	14.9	14.8	9.0
Series 3	14.0	15.8	16.8	11.0
Series 4	24.2	17.9	24.8	7.1
Series 5			17.4	9.1
Average*	17.1 ± 7.2	16.4 ± 1.3	18.1 ± 3.9	8.9 ± 1.4

*Error expressed as standard deviation when more than three series were performed

A2 CONTACT ANGLE

A2.1 CONTACT ANGLE OF AVR ASPHALTENES

Surface	Ni/Fe	Aluminum	Gold	Coke
Dynamic contact angle, °				
Series 1	77.0	65.9	61.5	46.2
Series 2	60.2	66.4	56.5	52.2
Series 3	62.2	68.8	55.2	56.8
Series 4	63.2	63.9		42.2
Series 5	56.4	65.2		42.4
Series 6	77.6	50.5		
Average*	66.1 ± 9.0	63.5. ± 6.6	57.7 ± 3.2	48.0 ± 6.4
Equilibrium contact angle, °				
Series 1	45.0			31.4
Series 2	43.1			29.0
Series 3	43.2			32.8
Series 4	36.3			25.9
Series 5	36.1			
Average*	40.7 ± 4.2			29.8 ± 3.0

*Error expressed as standard deviation when more than three series were performed

A2.2 CONTACT ANGLE OF MAYA VR ASPHALTENES

Surface	Ni/Fe	Aluminum	Gold	Coke
Dynamic contact angle, °				
Series 1	74.9			61.0
Series 2	75.7			60.7
Series 3	79.8			62.9
Series 4	78.9			64.8
Average*	77.3 ± 5.0			62.3 ± 1.9
Equilibrium contact angle, °				
Series 1	54.2			34.7
Series 2	61.0			24.4
Series 3	56.0			24.0
Series 4	55.5			
Average*	57.7 ± 3.3			27.7 ± 6.1

*Error expressed as standard deviation when more than three series were performed

A2.1 CONTACT ANGLE OF ARAB HEAVY VR ASPHALTENES

Surface	Ni/Fe	Aluminum	Gold	Coke
Dynamic contact angle, °				
Series 1	67.1			48.5
Series 2	64.2			53.5
Series 3	66.6			54.8
Series 4	71.8			53.1
Average*	67.4 ± 3.2			52.5 ± 2.7
Equilibrium contact angle, °				
Series 1	56.9			32.0
Series 2	49.8			34.4
Series 3	57.4			31.8
Series 4	50.0			27.1
Series 5	56.9			
Average*	54.2 ± 3.9			31.4 ± 3.1

*Error expressed as standard deviation when more than three series were performed

A2.1 CONTACT ANGLE OF GUDAO VR ASPHALTENES

Surface	Ni/Fe	Aluminum	Gold	Coke
Dynamic contact angle, °				
Series 1	60.3			63.5
Series 2	60.9			77.2
Series 3	59.3			61.3
Series 4	47.7			58.6
Average*	57.0 ± 6.3			65.2 ± 8.3
Equilibrium contact angle, °				
Series 1	28.8			18.8
Series 2	26.6			16.0
Series 3	26.6			15.3
Series 4	31.2			20.0
Series 5	27.7			18.3
Series 6	24.5			20.2
Series 7	31.4			
Series 8	27.2			
Series 9	28.8			
Average*	28.1 ± 2.2			17.7 ± 2.0

*Error expressed as standard deviation when more than three series were performed

APPENDIX B

KINETIC OF REACTION OF ASPHALTENES AND ASPHALTENES BLENDS

A generic expression of the form of Equation 1 was used to obtain a kinetic model for the depletion of the film thickness of the asphaltenes or VR/asphaltenes blends due to the thermal reactions. A first order kinetic model was considered partially based on the finding of Rahmani at al. (2002) for the modeling of the coke yield of the thermolysis of AVR/AVR asphaltenes

$$m = m_{t=\infty} + (m_{t=0} - m_{t=\infty}) * e^{-te_1} \qquad (1)$$

In Equation 1 m is the mass of the sample, the sub script t = ∞ and t = 0 represent final and initial stages, respectively; t is the reaction time, and e_1 is a kinetic constant. Equation 1 is properly bounded since:

At $t = 0 \rightarrow e^{-te_1} = 1$; Hence $m = m_{t=0}$, and

At $t = \infty \rightarrow e^{-te_1} = 0$; Hence $m = m_{t=\infty}$

To find the relation between the initial and final mass of the sample, several experimental runs were performed. Curie-point alloy rods were sprayed and uniformly coated with asphaltenes and vacuum residue/asphaltenes. Rods of known initial mass and film thickness were heated for different increasing times, until no further change of final mass was detected. The experiments were done at 400, 424, 466, 503, and 530 °C. For each temperature the average ratio between the final and initial mass was calculated as shown in Equation 2, where $X_{m,\ t=\infty}$ is the fraction of mass that remains in the rod no at t = ∞.

$$X_{m,t=\infty} = \frac{m_{t=\infty}}{m_{t=0}} \tag{2}$$

Combining Equations 1 and 2:

$$m = X_{m,t=\infty}\, m_{t=0} + (1 - X_{m,t=\infty}) m_{t=0} * e^{-te_1} \tag{3}$$

Now, using an expression similar to Equation 3-1, illustrated in Equation 4, the mass of the film on the rod can be changed by its film thickness. This approach assumes that the mass of the film on the rod is uniformly distributed along the same initial length (L = 10 mm). The terms of Equation 4 are the same as in Equation 3-1, except for m_{film} that stands for the mass of the thin film sprayed on the rod.

$$\delta = \frac{m_{film}}{\rho\,(2\pi R L)} * 10^5 \tag{4}$$

Combining Equations 3 and 4:

$$\delta\rho = X_{m,t=\infty}(\delta\rho)_{t=0} + (1 - X_{m,t=\infty})(\delta\rho)_{t=0} * e^{-te_1} \tag{5}$$

The term e_1 can be isolated from Equation 5 to obtain:

$$e_1 = -\frac{1}{t}\frac{\ln\left[\delta\rho - X_{m,t=\infty}(\delta\rho)_{t=0}\right]}{\ln\left[(1 - X_{m,t=\infty})(\delta\rho)_{t=0}\right]} \tag{6}$$

To calculate the constant e_1, the film thickness and the density of the coat must be known at the time t. To calculate the film thickness at a given time, the mass of the film remaining in the rod at that time must be known. Aminu (2003) reported data of the extent of cracking and volatilization of AVR as a function of time for several temperatures. These data can be used to calculate the remaining mass of asphaltenes on the rod after a time t based on the similar chemistry of the

asphaltenes and the whole vacuum residues. To verify the similarities between the vacuum residue and asphaltenes, the dry-out times for the asphaltenes where determined in another set of experiments. The dry-out times were compared to those from Aminu (2003), and gave good agreement.

Hence, the data from Aminu (2003) was used to calculate the fraction of extractable material converted at the dry-out time. The fraction unconverted was added to the un-extractable fraction of the initial mass (X) to calculate the total remaining mass on the rod. If the fraction of extractable material converted at a time t at a given temperature is X_{ext} , the total remaining mass on the rod as a function of the initial mass is given by Equation 7.

$$m_{film} = Xm_{t=0} + (1 - X_{m,t=\infty})(1 - X_{ext})m_{t=0} \qquad (7)$$

Having the total mass on the film, the only variable needed to calculate the film thickness at time t is the density. The density was estimated using Equation 8. This equation relates the density of the mixture (ρ_M) with the density of the liquid (ρ), the density of the solid (ρ_S), and the weight fraction of solids in the mixture (X_S). The weight fraction of solids in the mixture was assumed to be the fraction of coke formed at time t that for the lack of any other data was taken from Gray et al. (2004b). An average value of 0.1 was used for all the calculation, and thus assumed to be equivalent to the average fraction of coke to initial feed formed between 20 to 40 seconds at 503 °C. The density of the coke was assumed to be 1500 kg/m^3 (Gray, 2002) and for the density of the asphaltenes was used the same value of Section 3.4.1, 1200 kg/m^3.

$$\rho_M = \frac{\rho}{\left[1 - \frac{X_S}{\rho_S}(\rho_S - \rho)\right]} \tag{8}$$

Now Equation 4 can be applied and hence Equation 6 can be solved at the dry-out time to obtain the constant e_1 for a given temperature.

In parallel, Equation 5 can be rewritten as:

$$\delta = \delta_{t=0}\left[X_{m,t=\infty}\frac{\rho_{t=0}}{\rho_{t=\infty}} + (1 - X_{m,t=\infty})\frac{\rho_{t=0}}{\rho} * e^{-te_1}\right] \tag{9}$$

The density on the first term must be evaluated at t = ∞ because it represents the film thickness of the material at t = ∞. Taking the first term inside the brackets as a reference, and changing it according to Equation 10, shows that the condition shown in Equation 11 must be fulfilled for Equation 9 to be properly bounded at t = 0.

$$X_{m,t=\infty}\frac{\rho_{t=0}}{\rho_{t=\infty}} = e_2 \tag{10}$$

$$(1 - X_{m,t=\infty})\frac{\rho_{t=0}}{\rho} = 1 - e_2 \tag{11}$$

Combining Equations 9, 10 and 11:

$$\delta = \delta_{t=0}[e_2 + (1 - e_2) * e^{-te_1}] \tag{12}$$

that is the same expression shown in Equation 3-5

APPENDIX C

DETAILED EXPERIMENTAL PROCEDURES

C1 PREPARATION OF THE SAMPLES

C1.1 CONSTRUCTION OF THE ALLOY RODS-GLASS ROD ASSEMBLY

1. Each of the Curie-point rods was bent to a 45° shape as shown in Figure 3-1. The unbent portion was reduced by half for Curie-point rods of 300, 358, and 400 °C to prevent them from bending during pull apart because those rods are very soft.
2. The bent rods for the contact angle measurements (Curie-point 503 °C) were taken to the Machine shop where the bent portion was flattened to get a shape as shown in figure 3-2
3. The bent rods were then taken to the glass blower where a glass rod of diameter 3.9 mm and length 110 mm was firmly pressed to the longer unbent portion of the rod
4. The glass portion of the rod was then marked for identification with a glass engraver tool

C1.2 CHEMICAL ETCHING OF ALLOY RODS-GLASS ROD ASSEMBLY FOR SURFACE TENSION AND VISCOSITY MEASUREMENTS OF ASPHALTENES

1. A mixture of acetic acid, nitric acid, and acetone, 1:1:1 (v/v/v) was prepared in a glass beaker inside a fume hood.
2. The metallic part of the each of the flattened rods was cleaned with a paper towel soaked with methylene chloride. Then dried with a clean paper towel.

3. The metallic part of the each of the flattened rods was submerged in the acid mixture for 25-30 seconds, then completely dried with a clean paper towel

C1.3 COATING OF THE RODS FOR SURFACE TENSION AND VISCOSITY MEASUREMENTS

1. The marked glass rod was selected and weighed. Etched rods were used for the experiments with asphaltenes or vacuum residue/asphaltenes samples
2. The unbent portion of the rods were taped while exposing only the mid section of the Curie-point rod
3. A 2 wt % solution of the liquid (solid-free AVR, asphaltenes, a mixture of them or the calibration oil) was prepared with methylene chloride as solvent
4. The solution was then uniformly sprayed on the mid section of the Curie-point rods.
5. After spraying, the glass portion of the rod was cleaned with paper towel soaked in methylene chloride to ensure that only the desired portion was coated
6. The coated alloy was left inside a fume hood for at least 48 hours to ensure a that all the solvent was evaporated
7. After the 48 hours, the tape was carefully removed from the coated rods
8. The coated rod assembly was then weighed to determine the mass of liquid film on the rod
9. The film thickness on the rod was calculated based on Equation 3-1

10. Taping, weighing and spraying steps were repeated with drying out in between until the desired film thickness was obtained

C1.4 COATING OF THE RODS FOR CONTACT ANGLE MEASUREMENTS WITH COKE

1. The marked glass rod was weighed
2. The unbent portion of the rods were taped while exposing only the mid section of the Curie-point rod
3. A 2 wt % solution of AVR was prepared with methylene chloride as solvent
4. The solution was then uniformly sprayed on the mid section of the flattered rods until the surface was completely covered with a thick film of the solution.
5. After spraying, the glass portion of the rod was cleaned with paper towel soaked in methylene chloride to ensure that only the desired portion was coated
6. The coated alloy was left inside a fume hood for at least 48 hours to ensure a that all the solvent was evaporated
7. After the 48 hours, the tape was carefully removed from the coated rods
8. The coated rod assembly was then attached to the lower aluminum bean the apparatus shown in Figure 3-3
9. The apparatus was then closed by attaching the glass housing
10. The glass housing part of the device was placed inside the coil of the induction furnace

11. The apparatus was then flushed with a flow of 9-10 dm^3/min of nitrogen for 10 minutes
12. After the 10 minutes of flushing the induction furnace was turned on at the maximum heating rate for 180 seconds, then the furnace was switched off
13. After the 180 seconds of heating (at circa 500 °C) the rod was left cooling down for 120 seconds and then taken from the aluminum bean and stored
14. The same procedure was repeated for all the flattened rod to be coated with coke

C1.5 COATING OF THE RODS FOR CONTACT ANGLE MEASUREMENTS WITH GOLD AND ALUMINUM

1. The rods were carefully cleaned with toluene, then air-dried
2. The rods were then cleaned with methylene chloride and also air-dried
3. The rods were taken to the Micromachining and Nanofabrication facility to be coated with the metals.
4. At this facility, some rods were coated with gold and some others with aluminum. Both coatings were done using a sputter machine

C2 SURFACE TENSION AND VISCOSITY MEASUREMENTS

1. Two rods coated with the same material at a desired film thickness and of the same Curie-point temperature were loaded on the equipment as shown in Figure 3-3
2. LabView program was started for the control of the stepper motor that moved the controlled rod and the visualization of the voltage signals from the LVDTs
3. From LabView, the predesigned program "LesD.vi" was opened in an inactive mode
4. To make the program active, the "start" button was clicked followed by the "on/off" button and finally the "run" button, which is a white arrow symbol on the menu of the program and "save file" window appears to save the data from the run
5. The file "test" was saved and made the program active giving the graphical display of the responses from the two LVDTs and the program allowed the stepper motor to have the controlled (lower) rod moved up till it just touched the free rod
6. The step rate was set to 100, which corresponds to 4148 steps/second or 0.4086 mm/s
7. The counterweight was adjusted such that the free (upper) rod was positioned within the range of the LVDT1 and the controlled rod within

the range of the LVDT2, both with enough room to move down 80,000 steps

8. From the touch point, the controlled rod was moved down a predetermined number of steps depending on the reaction time desired. (For example for reaction time of 15 seconds, the lower rod was moved down 60,000 steps while using minimum step rate of 100, which implied a rate of approximately 4000 steps per second)
9. The LabView program was closed
10. After all the glass fittings were properly sealed, the front side of the equipment was connected to the nitrogen purge line through the flow meter and the rear side was connected to the nitrogen supply line
11. The nitrogen cylinder was opened fully to allow for flow of nitrogen
12. The test-utility program was opened (via start/programs/Advantech Driver for 95 and 98/Test Utility) to control the opening of the valve on the nitrogen line
13. The pre-designed file "PCL-7330-I/O = 300H" was opened and started to open the valve on the nitrogen line and begin the flow of nitrogen
14. The flow of nitrogen was monitored on the flow meter with the stopwatch while the valve on the nitrogen cylinder was adjusted till a flow-rate of 9-10 dm^3/min was obtained
15. When this flow-rate was attained, the test-utility program was closed

16. The glass housing portion of Figure 3-3 was then inserted into the induction coil of the furnace
17. The lighting was set to the appropriate position to provide illumination for the enhancement of the video recordings
18. The rods were brought into the view of the camera such that the experiments could be recorded into a videotape and afterwards the lighting was turned off
19. The front end of the equipment was removed from the flow meter and connected directly to the nitrogen purge line while every other setting remained the same
20. The GeniDAQ runtime program was opened (via Start/programs/Advantech GeniDAQ/GeniDAQ runtime) to control the operation of the valve on the nitrogen line and that of the induction furnace
21. The pre-designed file "p20-300s.gni" was opened to reopen the nitrogen line and purge the equipment with nitrogen for 20 minutes, and immediately afterwards, to turn on the furnace for 300 seconds
22. The program was started and purging of the equipment with nitrogen began. The stop watch was started to synchronized the time of the equipment to allow for the necessary moving around for the experiment
23. At this point the circulation fan was switched-on to ensure the circulation of the nitrogen

24. 17 minutes into the purging, the power supply for the furnace was switched on, thought the induction furnace was still off till the GeniDAQ runtime turned it on at the end of purging time of 20 minutes

25. At this time the heating rate control of the induction furnace was verified to be set at the highest heating rate, it is a set point of 38.1

26. 18.5 minutes into the purging, LabView program was restarted as explained in steps 2 to 6, but this time, a different name was given to the file into which the data from the experiment would be saved

27. The nudge amount was set, on the LabView program interface to 65,105 steps (60,000 steps of separation plus 5,105 steps for press together)

28. 19 minutes into the purging, the nitrogen was turned low to ca. 1-2 dm^3/min and the circulation fan was switched-off to reduce the oscillation of the free rod

29. To obtain the desired nudge action on LabView, the "set parameter" button was clicked, the "move absolute" position set to zero and the "set" button clicked

30. 19.5 minutes into the purging, the lights were turned on and the VCR is set to record

31. At exactly 20 minutes after purging started, the induction furnace automatically came on and heating of the rod started

32. The "run/stop" button in the "take-measurement" was clicked as desired to start the nudge action of the rods. This action also starts the timer which stamps the time on the videotape

33. Clicking the "run/stop" button initiated the nudge, press together and pull apart of the rod and the green color of the button indicated the execution of the nudge command

34. After the nudge, pull apart, bridge formation and elongation were completed, the stepper motor stopped to indicate the end of the experiment

35. At the end of the experiment, the lights were switched off and the VCR stopped from recording, the LabView program stopped by clicking the "stop", "exit" and "on/off" buttons in that order

36. Pressing the red button stopped the furnace and the GeniDAQ program stopped by clicking the stop button. The furnace power was switched off and the nitrogen cylinder closed

37. The experiment was completed by saving the data file in a removable disk for further processing on another computer

38. The rods were cleaned with abrasive and solvent and reused for other experiments

C3 CONTACT ANGLE MEASUREMENTS

1. One flattened rod coated with the desired material was selected and a 30-gauge type K thermocouple wire was spot-welded underneath the bent portion
2. The rods was then attached to the lower aluminum beam of the equipment shown in Figure 3-3
3. The thermocouple was connected to a Benchlink Data Logger
4. The equipment was moved placing the rod inside the coil of the induction furnace
5. The lighting was set to the appropriate position to provide illumination for the enhancement of the video recordings
6. The rods were brought into the view of the camera and the bent (flattened) portion of the rod was set in an horizontal plane with the help of the enlarged image on the TV
7. Afterwards the lighting was turned off and the rod moved out of the coil of the induction furnace
8. Two or three particles of the desired asphaltenes were carefully place equally separated on the bent portion of the rod
9. The glass fittings were properly sealed, the front side of the equipment was connected to the nitrogen purge line through the flow meter and the rear side was connected to the nitrogen supply line
10. The nitrogen cylinder was opened fully to allow for flow of nitrogen

11. The test-utility program was opened (via start/programs/Advantech Driver for 95 and 98/Test Utility) to control the opening of the valve on the nitrogen line
12. The pre-designed file "PCL-7330-I/O = 300H" was opened and started to open the valve on the nitrogen line and begin the flow of nitrogen
13. The flow of nitrogen was monitored on the flow meter with the stopwatch while the valve on the nitrogen cylinder was adjusted till a flow-rate of 9-10 dm^3/min was obtained
14. When this flow-rate was attained, the test-utility program was closed
15. The glass housing portion of Figure 3-3 was then inserted into the induction coil of the furnace
16. The lighting was set to the appropriate position to provide illumination for the enhancement of the video recordings
17. The rod was brought into the view of the camera such that the experiments could be recorded into a videotape, and afterwards the lighting was turned off
18. The front end of the equipment was removed from the flow meter and connected directly to the nitrogen purge line while every other setting remained the same
19. The GeniDAQ runtime program was opened (via Start/programs/Advantech GeniDAQ/GeniDAQ runtime) to control the

operation of the valve on the nitrogen line and that of the induction furnace

20. The pre-designed file "p10-300s.gni" was opened to reopen the nitrogen line and purge the equipment with nitrogen for 10 minutes, and immediately afterwards, to turn on the furnace for 300 seconds
21. The program was started and purging of the equipment with nitrogen began. The stop watch was started to synchronized the time of the equipment to allow for the necessary moving around for the experiment
22. At this point the circulation fan was switched-on to ensure the circulation of the nitrogen
23. 8 minutes into the purging, the power supply for the furnace was switched on, thought the induction furnace was still off till the GeniDAQ runtime turned it on at the end of purging time of 10 minutes
24. At this time the heating rate control of the induction furnace was verified to be set at the lowest heating rate, it is a set point of -5.0
25. 8.5 minutes into the purging, the program to the temperature data acquisition was started (via Start/Programs/BenchLink/HP Benchlink Data Logger)
26. 9 minutes into the purging, the nitrogen was turned low to ca. 1-2 dm^3/min and the circulation fan was switched-off to avoid cooling of the rod or samples by the flow of nitrogen

27. 19.5 minutes into the purging, the lights were turned on and the VCR is set to record

28. At exactly 10 minutes after purging started, the induction furnace automatically came on and heating of the rod started

29. At the same time the "start" button on the front panel of the timer was pressed to star the timer which stamps the time on the videotape

Dynamic Contact Angle Measurements

30. The heating was kept until the first signs of reaction (bubbling) were observed on the TV screen. At this point the lights were switched off and the VCR stopped from recording

31. Pressing the red button stopped the furnace and the GeniDAQ and Benchlink Data Logger programs stopped by clicking the stop button. The furnace power was switched off and the nitrogen cylinder closed

32. The experiment was completed by saving the temperature data file in a removable disk for further processing on another computer

Equilibrium Contact Angle Measurements

30. The increasing heating of the samples was kept until a temperature of 270 °C was reached (observed on the monitor of the personal computer)

31. At this point a temperature of 270 ± 5 °C was maintained by continuously pressing the on and off buttons on the induction furnace control. The constant temperature was maintained for a total heating time of 180 seconds (controlled in the stopwatch)

32. At this point the lights were switched off and the VCR stopped from recording.

33. Pressing the red button stopped the furnace and the GeniDAQ and Benchlink Data Logger programs stopped by clicking the stop button. The furnace power was switched off and the nitrogen cylinder closed

34. The experiment was completed by saving the temperature data file in a removable disk for further processing on another computer